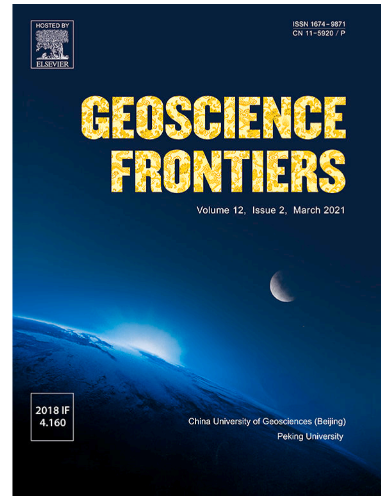

Research Paper

Evaluation and comparison of CMIP6 models and MERRA-2 reanalysis AOD against Satellite observations from 2000 to 2014 over China

Arfan Ali, Muhammad Bilal, Yu Wang, Zhongfeng Qiu, Janet E. Nichol, Gerrit de Leeuw, Song Ke, Alaa Mhawish, Mansour Almazroui, Usman Mazhar, Birhanu Asmerom Habtemicheal, M. Nazrul Islam

PII: S1674-9871(21)00189-4
DOI: https://doi.org/10.1016/j.gsf.2021.101325
Reference: GSF 101325

To appear in: *Geoscience Frontiers*

Received Date: 24 June 2021
Revised Date: 4 November 2021
Accepted Date: 8 November 2021

Please cite this article as: A. Ali, M. Bilal, Y. Wang, Z. Qiu, J.E. Nichol, G. de Leeuw, S. Ke, A. Mhawish, M. Almazroui, U. Mazhar, B. Asmerom Habtemicheal, M. Nazrul Islam, Evaluation and comparison of CMIP6 models and MERRA-2 reanalysis AOD against Satellite observations from 2000 to 2014 over China, *Geoscience Frontiers* (2021), doi: https://doi.org/10.1016/j.gsf.2021.101325

Research Paper

Evaluation and comparison of CMIP6 models and MERRA-2 reanalysis AOD against Satellite observations from 2000 to 2014 over China

Md. Arfan Ali[a], Muhammad Bilal[a], Yu Wang[a], Zhongfeng Qiu[a,*], Janet E. Nichol[b], Gerrit de Leeuw[c,d,e,f], Song Ke[g], Alaa Mhawish[a], Mansour Almazroui[h,i], Usman Mazhar[j], Birhanu Asmerom Habtemicheal[k,l], M. Nazrul Islam[h]

[a] Lab of Environmental Remote Sensing (LERS), School of Marine Sciences, Nanjing University of Information Science and Technology, Nanjing 210044, China.

[b] Department of Geography, School of Global Studies, University of Sussex, Brighton BN19RH, UK.

[c] Royal Netherlands Meteorological Institute (KNMI), R & D Satellite Observations, 3730AE De Bilt, The Netherlands.

[d] School of Atmospheric Physics, Nanjing University of Information Science and Technology, Nanjing 210044, China.

[e] Aerospace Information Research Institute, Chinese Academy of Sciences (AirCAS), No.20 Datun Road, Chaoyang District, Beijing 100101, China.

[f] School of Environment Science and Spatial Informatics, University of Mining and Technology, Xuzhou, Jiangsu 221116, China

[g] Geological Survey of Jiangsu Province, Nanjing 210018, China

[h] Center of Excellence for Climate Change Research/Department of Meteorology, King Abdulaziz University, Jeddah 21589, Saudi Arabia

[i] Climatic Research Unit, School of Environmental Sciences, University of East Anglia, Norwich, UK.

[j] School of Remote Sensing and Geomatics Engineering, Nanjing University of Information Science and Technology, Nanjing 210044, China

[k] School of Atmospheric Physics, Nanjing University of Information Science and Technology, Nanjing 210044, China

[l] Department of Physics, Wollo University, Dessie P.O. Box 1145, Ethiopia

[*] Corresponding author's email: zhongfeng.qiu@nuist.edu.cn

Handling Editor: R. Palin

Abstract

Rapid industrialization and urbanization along with a growing population are contributing significantly to air pollution in China. Evaluation of long-term aerosol optical depth (AOD) data from models and reanalysis, can greatly promote understanding of spatiotemporal variations in air pollution in China. To do this, AOD (550 nm) values from 2000 to 2014 were obtained from the Coupled Model Inter-comparison Project (CIMP6), the second version of Modern-Era Retrospective analysis for Research, and Applications (MERRA-2), and the Moderate Resolution Imaging Spectroradiometer (MODIS; flying on the Terra satellite) combined Dark Target and Deep Blue (DTB) aerosol product. We used the Terra-MODIS DTB AOD (hereafter MODIS DTB AOD) as a standard to evaluate CMIP6 Ensemble AOD (hereafter CMIP6 AOD) and MERRA-2 reanalysis AOD (hereafter MERRA-2 AOD). Results show better correlations and smaller errors between MERRA-2 and MODIS DTB AOD, than between CMIP6 and MODIS DTB AOD, in most regions of China, at both annual and seasonal scales. However, significant under- and over-estimations in the MERRA-2 and CMIP6 AOD were also observed relative to MODIS DTB AOD. The long-term (2000–2014) MODIS DTB AOD distributions show the highest AOD over the North China Plain (0.71) followed by Central China (0.69), Yangtse River Delta (0.67), Sichuan Basin (0.64), and Pearl River Delta (0.54) regions. The lowest AOD values were recorded over the Tibetan Plateau (0.13 ± 0.01) followed by Qinghai (0.19 ± 0.03) and the Gobi Desert (0.21 ± 0.03). Large amounts of sand and dust particles emitted from natural sources (the Taklamakan and Gobi Deserts) may result in higher AOD in spring compared to summer, autumn, and winter. Trends were also calculated for 2000–2005, for 2006–2010 (when China introduced strict air pollution control policies during the 11th Five Year Plan or FYP), and for 2011–2014 (during the 12th FYP). An increasing trend in MODIS DTB AOD was observed throughout the country during 2000–2014. The uncontrolled industrialization, urbanization, and rapid economic development that mostly occurred from 2000 to 2005 probably contributed to the overall increase in AOD. Finally, China's air pollution control policies helped to reduce AOD in most regions of the country; this was more evident during the 12th FYP period (2011–2014) than during the 11th FYP period (2006–2010). Therefore this study strongly advises the authority to retain or extend these policies in the future for improving air quality.

Keywords: AOD, CMIP6, MERRA-2, MODIS, Trends

1. Introduction

Aerosols are mixtures of tiny solid and liquid suspended particles in the atmosphere, having a standard radius from 0.001 to 100 μm. Aerosols are of great interest to the scientific community due to their impact on global climate, radiative balance, air quality, human health, cloud microphysical properties, hydrological cycle, ecosystems, and agriculture (Charlson et al., 1992; Xia et al., 2006; Yu et al., 2009; Wang et al., 2015; You et al., 2015; Shao et al., 2017). Several studies on this topic have been conducted over different regions around the world to understand aerosol behavior (Che et al., 2009, 2015a, 2015b; Zhang et al., 2012; Bilal and Nichol, 2015, 2017; Kong et al., 2016; Ma et al., 2016; Xin et al., 2016; Bilal et al., 2017a, 2017b, 2018; Ali et al., 2019, 2020; Zhang et al., 2020; Su et al., 2021). Even so, aerosol optical properties remain an important source of uncertainty in climate projection and assessment (IPCC, 2013). Aerosol optical depth (AOD) is an essential parameter that measures aerosol loading in the atmosphere and is a principal factor for climate change research (Pan et al., 2010). Therefore, AOD evaluation at local to global scales, its long-term spatiotemporal variations, and trend calculations, are necessary, and especially in China which has severe air pollution.

Such analysis requires multiple datasets (e.g., ground measurements, satellite remote sensing, reanalysis, and model simulation) for a comprehensive understanding of the nature and effects of aerosols. National Aeronautics and Space Administration (NASA) Aerosol Robotic Network (AERONET) (Holben et al., 1998), in 2001. Complementary to AERONET, and in part shared with AERONET, Chinese networks have been developed (Xia et al., 2021), such as CARSNET (China Aerosol Remote Sensing Network), established by the China Meteorological Administration (CMA) (Che et al., 2009, 2015a) (50 sites), and SONET (Sun-Sky Radiometer Observation Network) established by the Institute of Remote Sensing and Digital Earth, Chinese Academy of Sciences (RADI/CAS), Beijing (Li et al., 2018) (16 sites). CARE China (Campaign on Atmospheric Aerosol Research network of China) (Xin et al., 2015) includes 36 sites where handheld sun photometers are used. The limitation of these networks is their sparse spatial distribution (Holben et al., 2001). This limitation can be overcome by satellite remote sensing techniques and Global Climate Models (GCMs), which provide wide spatial coverage of AOD at local to global scales. AOD retrievals are available from several satellite-based instruments such as the Total Ozone Monitoring Instrument (TOMS) (Torres et al., 2002), Advanced Very High-Resolution Radiometer (AVHRR) (Hauser, 2005), the Along Track Scanning Radiometers (ATSR-2 and AATSR) (Holzer-Popp et al., 2013; de Leeuw et al., 2015; Popp et al., 2016), Ozone Monitoring Instrument (OMI) (Torres et al., 2007), Multi-angle Imaging Spectroradiometer (MISR) (Kahn et al., 2010), the Sea-Viewing Wide-field of View Sensor (SeaWiFS) (Sayer et al., 2012), the Visible Infrared Imaging Radiometer Suite (VIIRS) (Liu et al., 2014), and the Moderate Resolution Imaging Spectroradiometer

(MODIS) (Remer et al., 2005; Hsu et al., 2006, 2013; Levy et al., 2010, 2013; Sayer et al., 2014). In addition, reanalysis data such as from Copernicus Atmosphere Monitoring Services (CAMS) (Flemming et al., 2017), the second Modern-Era Retrospective analysis for Research and Applications (MERRA-2) (Randles et al., 2017), and Global Climate Models (GCMs) such as the Coupled Model Intercomparison Project Phase6 (CMIP6) (Eyring et al., 2016) also provide long-term spatial AOD data.

MODIS, onboard the Terra and Aqua satellites is one of the most widely appraised instruments in retrieving AOD (Levy et al., 2013; Sayer et al., 2014; Bilal and Nichol, 2015; Mhawish et al., 2017). The satellite-based MODIS sensor provides global AOD distributions using the dark target (DT) and deep blue (DB) algorithms, which have been widely evaluated over vegetated and bright reflecting surfaces (Kaufman et al., 1997; Hsu et al., 2013). In addition, several researchers evaluated the MODIS DT, DB, and their combined DTB AOD products over different regions (Chu et al., 2002; Bilal et al., 2016, 2017b, 2018, 2021a; Georgoulias et al., 2016; Nichol and Bilal, 2016; Ali et al., 2017; Butt et al., 2017; Mhawish et al., 2017; Wang et al., 2017; de Leeuw et al., 2018; Sogacheva et al., 2018, 2020; Ali and Assiri, 2019; Almazroui, 2019; Bright and Gueymard, 2019; Mei et al., 2019; Tian and Gao, 2019; Filonchyk and Hurynovich, 2020; Wei et al., 2020). Apart from these, several studies also evaluated MODIS AOD products against ground measurements in different regions of China. For example, Wang et al. (2019) evaluated MODIS collection (C6.1) DT and DB AOD against 20 AERONET sites over different regions in China and reported that DB performed well to estimate AOD in terms of correlation coefficient (r = 0.931), root mean squared error (RMSE = 0.18), relative mean bias (RMB = 1.02), and an acceptable percentage of retrievals within the expected error (EE = 63.49%). The corresponding DT values were r = 0.946, RMSE = 0.19, RMB = 1.17, and EE = 54.03%. The MODIS C6.1 DB AOD performed better against AERONET AOD measurements over Beijing, XiangHe, and Xinglong sites as indicated by r (0.92), RMSE (0.22), and EE (68.3%) compared to the DT algorithm (Bilal et al., 2019). Huang et al. (2020) evaluated Terra and Aqua based MODIS C6.1 DT and DB AOD against SONET sites in the westernmost city (Kashi region, Xinjiang Uygur Autonomous Region) in China and reported that DB showed better results for both satellites in terms of r (Terra/Aqua = 0.896/0.907), RMSE (0.283/0.203), RMB (0.337/0.388), and EE (82.35/84.06%) compared to the DT algorithm. In addition, Che et al. (2019a) validated MODIS C6 and C6.1 DT AOD over 18 AERONET and CARSNET sites in China for the period 2002 to 2014. They found that DT C6.1 obtained better results in retrieving AOD in terms of r (0.901), RMSE (0.171), RMB (0.998), and EE (59.03%) compared to the C6 DT algorithm (r = 0.890, RMSE = 0.185, RMB = 1.039, EE = 54.94%). Huang et al. (2019) validated MODIS C006 and 61 DT AOD 3km products against AERONET sites in China, and they reported that C6.1 DT performed better in terms of R^2 (0.87), RMSE (0.23), RMB (1.41), and EE (45%) than did C6 DT (0.81, 0.31, 1.57, and 39%). Apart from these, Li et al. (2020) reported that the C6.1 MODIS DTB AOD product produced better results over 12 AERONET sites in China as indicated by R^2 (Terra/Aqua = 0.81/0.79), RMSE (0.15/0.17), and EE (66.63/65.32%) compared to the DT and DB algorithms. The DTB AOD product also has good spatial coverage over multilayer surfaces in China. Filonchyk et al. (2019) used this product for a local study and found that the combined C6.1 MODIS DTB AOD performed better over four AERONET sites (Beijing, XiangHe, Taihu, and SACOL), as indicated by r (0.885–0.902), RMSE (0.097–0.302), RMB (0.97–1.17), and EE (76.3%–78.3%). Based on the good performance of the DTB AOD retrievals over China, as reported by previous studies, the present study used the combined Terra-MODIS C6.1 DTB AOD as the reference data to evaluate CMIP6 and the MERRA-2 AOD.

Very few studies were found that evaluated CMIP5/CMIP6 models and MERRA-2 reanalysis-based AOD against satellite observations from local to global scales. Mortier et al. (2020) calculated AOD trends using the CMIP6 and AeroCom models at a global scale and reported decreasing trends in AOD over Europe, North and South America, and North Africa. Li et al. (2020) evaluated the CMIP5 model-based AOD against MODIS AOD over East Asia from 2001 to 2005 and reported an underestimation in CMIP5 AOD. Similar studies were conducted by Misra et al. (2016) and Sockol and Small Griswold (2017) over the USA and India, respectively. In China, Sun et al. (2019) evaluated the MERRA-2 reanalysis AOD against Aqua-based MODIS AOD from 1980 to 2010 and Liu et al. (2021) evaluated CAMS and MERRA-2 AOD against MODIS AOD over the Sichuan Basin of China. However, no comprehensive evaluation of MERRA-2 and CMIP6 AOD data was found over China. Due to the unprecedented social and economic developments of China in recent decades, the country now suffers from intense aerosol pollution (Wang et al., 2021). In 2015, a total of 1710 days of severe and above pollution, and 154 heavy pollution weather warnings were observed across 70 cities in the BTH region. In 2016, Yale University published the Environmental Performance Index (EPI) report, which ranked China as having the second worst air quality globally, before Bangladesh (Song et al., 2019; Qiu et al., 2021). For the use of MERRA-2 reanalyses and CMIP6 AOD for air quality assessments, a comprehensive evaluation of the model results is required to see how well they represent the local to regional spatio-temporal AOD scenarios and trends over China. In this contribution, the model results are evaluated against MODIS AOD. The main objectives of this study are: (1) to evaluate CMIP6 Ensemble AOD and MERRA-2 reanalysis AOD against Terra-MODIS AOD; (2) investigate the long-term spatiotemporal discrepancy of AOD at annual and seasonal scales; and (3) to estimate the effect of China's air pollution control policies on AOD.

2. Data and methods

2.1 Study area

In this study, AOD from multiple sources was investigated over China. China is characterized by having a diverse climate and broad geography, and is located at 3°51′−53° 33′ N latitudes and 73°33′−135° 05′ E longitudes (Fig. 1). China's regions have a large landmass with a complex topography and aerosol heterogeneity. Climatologically, China's climate varies from south and southeast (humid) to north and northwest (dry), with an uneven pattern of precipitation, which is mainly due to the distance from the sea. The northern and western regions of the country are dominated by the Gobi and Taklamakan Deserts with plateaus and massifs, whereas the southern regions comprise hilly and mountainous terrain. The southern coastal and eastern plains are composed of fertile lowlands and foothills, and so the largest number of people live in these regions. The country has four distinct seasons. December to February (DJF) represent a harsh cold winter with a very dry climate in most of China, except for southern China, which remains just cool. A more moderate climate occurs in spring from March to May (MAM), while the summer months June to August (JJA) brings are very hot and humid. The autumn lasts from September to November (SON) and is characterized by warm weather with strong winds and infrequently heavy rain.

In China, aerosol distribution varies over time and from region to region; therefore a region-based study is more effective in distinguishing the long-term changes in aerosols compared to the national scale (Zhao et al., 2008). Emissions from different industries located in different regions are key sources of aerosol in China. Industrial aerosols are emitted mostly from the Eastern (Pan et al., 2010; Deng et al., 2012; He et al., 2016; Kang et al., 2016a, 2016b) and Central (Wang et al., 2015; Liu et al., 2016) part of China. In addition, dust aerosols across the Northern and Northwestern regions of China are triggered by wind erosion (Tan et al., 2015; Yu et al., 2016). Marine aerosols found over the Eastern and Southern parts of China are generated from the Yellow Sea and the South China Sea (Kang et al., 2016a). In light of the above, ten major regions (see Fig.1) were selected across China. Results for the ten regions are amalgamated to calculate results for an 11^{th} region "Entire China", representing the whole of China.

2.2 Aerosol products

2.2.1 CMIP6 based AOD datasets

In this study, we used multi-model historical simulations from the latest CMIP6 archive, which extend up to 2014. Trends in AOD at 550 nm for the 10 selected regions in China were investigated for the 2000–2014 simulation period. In this regard, we used AOD data from 15 CMIP6 up-to-date global climate models (GCMs). Based on the availability of required data, output from those 15 models was downloaded from the CMIP6 website. Some details of the selected 15 GCMs are summarized in Table 1.

2.2.2 MERRA-2 reanalysis AOD datasets

In this study, the reanalysis AOD from MERRA-2 at a spatial resolution of 0.5° × 0.625° was used. MERRA-2 is the updated version of the original MERRA reanalysis datasets (Rienecker et al., 2011). The inclusion of the Goddard Earth Observing System (GEOS) model, as well as the assimilation of observation types, is the fundamental enhancement in this upgraded version (Molod et al., 2015; Georgoulias et al., 2016; Gelaro et al., 2017). MERRA-2 is recognized as the first satellite reanalysis product to assimilate aerosol information for the earth system. It represents the interaction between aerosols and climate system variables on the Earth. The aerosol model is developed based on the assimilation of AOD products from the Advanced Very High-Resolution Radiometer (AVHRR), MISR (Multi-angle Imaging Spectroradiometer), and MODIS satellite-based sensors, as well as from ground-based observations such as provided by AERONET (Aerosol Robotic Network). For more details about MERRA-2 and the evaluation of aerosol assimilation, see Gelaro et al. (2017), Randles et al. (2017), and Shi et al. (2019).

2.2.3 MODIS AOD datasets

This study also used the MODIS aerosol products, as they have the greater availability of effective AOD pixels (de Meij et al., 2012; de Leeuw et al., 2018). To explore the spatiotemporal features of aerosols, MODIS was launched in 1999 onboard the Terra (descending orbit, local crossing time: 10:30 AM) satellite and in 2002 onboard the Aqua (ascending orbit, local crossing time: 01:30 PM) satellite as part of NASA's Earth Observing System (EOS) mission. This sensor measures the upwelling Earth radiation in 36 spectral channels from 0.4–14.4 μm and with three different spatial resolutions (e.g., 250 m for bands 1–2, 500 m for bands 3–7, 1 km for 8–36) with a swath viewing of 2330 km (for details see https://modis.gsfc.nasa.gov/about/specifications.php; accessed date: 22 Feb 2021). To retrieve MODIS AOD, three different algorithms, i.e. the dark target (DT) land algorithm, the dark target (DT) ocean algorithm, and the deep blue (DB) land algorithms are used (Hsu et al., 2013; Levy et al., 2013; Remer et al., 2013). The DT algorithm is applicable for vegetated surfaces, whereas the DB algorithm is used for both bright reflecting (desert surface) and vegetated surfaces. However, based on upgrades to the algorithms, MODIS AOD datasets are stored at different levels and versions (known as collections). The collection (C6.1) is the latest version of DT and DB algorithms, where significant improvements and modifications were implemented from the previous C51 and C6 versions (Levy et al., 2013; Bilal and Nichol, 2015; Bilal et al., 2016; Georgoulias et al., 2016; Nichol and Bilal, 2016), as described in Sayer et al. (2019) and initially validated over China by Sogacheva et al. (2018). This study used combined MODIS AOD products, considering their reliability and extended coverage in terms of the enormous number of valid pixels and their quality in retrieving AOD over both land and ocean surfaces (Levy et al., 2013; Sayer et al., 2014). The MODIS C6.1 combined DT and DB (DTB) monthly AOD (at 550 nm), from the Terra satellite with a spatial resolution of 1° × 1°, was obtained from NASA Giovanni (https://giovanni.gsfc.nasa.gov/giovanni/; accessed date: 20 December 2020). Several studies were also used level 3 MODIS DTB AOD with a spatial resolution of 1° × 1° to investigate air pollution scenario (Ali and Assiri, 2016; Ali et al., 2017, 2019; de Leeuw et al., 2018; Nichol et al., 2020; Qiu et al., 2021). More detailed statistics about MODIS, its products, calibration process, retrieval algorithms, and associated uncertainties have been discussed elsewhere (Levy et al., 2015; Sayer et al., 2015; Georgoulias et al., 2016; Bilal et al., 2017b, 2018; Bilal and Nichol, 2017; de Leeuw et al., 2018; Ali and Assiri, 2019). Henceforth, the Terra MODIS C6.1 combined DTB product is referred to as MODIS DTB AOD.

2.3 Research Methodology

We followed these step-by-step methods to achieve our objectives:

- The AOD obtained from 15 CMIP6 models, MERRA-2 reanalysis, and Satellite (Terra MODIS DTB) was interpolated onto the same geographical grid (0.5° × 0.5°) using the bilinear interpolation technique (Yousefi et al., 2020; Wang et al., 2021) in the Climate Data Operators (CDO) tool.

- To reduce the differences among the 15 CMIP6 models and ensure the accuracy of AOD changes, a new AOD dataset (i.e., CMIP6 Ensemble) was generated from the combination of 15 CMIP6 models using the CDO tool. The study used a nearest interpolation technique using MATLAB software to remove the data gaps that affect the results and analysis of the MODIS AOD products (Yang and Hu, 2018).
- Several statistical methods were used to evaluate the CMIP6 and MERRA-2 AOD against MODIS DTB AOD. The methods are as follow:

The linear regression technique (Wilks, 2007) was used to calculate slope, intercept, and significance (Eq. (1)):

$$Y = mx + c \quad (1)$$

where Y is the linear estimate, m defines the slope (a change of Y per unit changes of x), and c indicates the intercept or constant. The slope value is defined as the trend of the CMIP6, MERRA-2, and MODIS-DTB based AOD. Trend significance is estimated based on the p-value (a null hypothesis) (Ali et al., 2019). A p-value less than or equal to (≤ 0.05) is defined as significant with a 95% confidence level, while $p > 0.05$ indicates statistically insignificant. In addition, to calculate the uncertainty of CMIP6 and MERRA-2 AOD, we used the Pearson's correlation (r), root mean squared error (RMSE), mean absolute error (MAE), relative mean bias (RMB) (Bilal et al., 2016, 2021a, 2021b; Ali and Assiri, 2019; Almazroui, 2019; Islam et al., 2019)

$$r = \frac{\sum_{i=1}^{n}(x_i - \bar{x})(y_i - \bar{y})}{\sqrt{\sum_{i=1}^{n}(x_i - \bar{x})^2 \sum_{i=1}^{n}(y_i - \bar{y})^2}} \quad (2)$$

$$\mathrm{RMSE} = \sqrt{\frac{1}{n}\sum_{i=1}^{n}(\text{Model AOD} - \text{MODIS DTB AOD})^2} \quad (3)$$

$$\mathrm{MAE} = \frac{1}{n}\sum_{i=1}^{n}\left|(\text{Model AOD} - \text{MODIS DTB AOD})\right| \quad (4)$$

$$\mathrm{RMB} = \left(\frac{\text{Model AOD} - \text{MODIS DTB AOD}}{\text{MODIS DTB AOD}}\right) \quad (5)$$

where Model = CMIP6 and MERRA-2, RMB = 1 defines the normal estimation of CMIP6 and MERRA-2, and positive and negative values represent over- and underestimations, respectively.

- Spatial and area-averaged maps of mean annual and seasonal AOD were generated from monthly CMIP6, MERRA-2, and MODIS DTB AOD from 2000−2014.

3. Results and discussion

3.1 Evaluation of CMIP6 and MERRA-2 AOD against MODIS DTB AOD

Figure 3 shows that the better performance of the MERRA-2 AOD with respect to the MODIS DTB AOD, than that of the CMIP6 Ensemble AOD. The MERRA-2 statistical measures showed higher correlation (r = 0.71–0.89) and lower error (RMSE = 0.07–0.23, MAE = 0.05–0.17) than that of the CMIP6 Ensemble AOD with a lower correlation (r = 0.38–0.66) and higher error (RMSE = 0.05–0.28, MAE = 0.04–0.23) over all regions as well as for Entire China. In terms of RMB, both datasets underestimated AOD (MERRA-2 = −0.05 to −0.22, CMIP6 = −0.05 to −0.30) over the Northeast, North China Plain, and Pearl River Delta and overestimate AOD (MERRA-2 = 0.11, CMIP6 = 0.53) over the Gobi Desert except for the Tibetan Plateau. MERRA-2 performed better than CMIP6, with moderate correlations (r = 0.51–0.64) and errors (RMSE = 0.11–0.20, MAE = 0.08–0.15) over the Yangtse River Delta, Central, Qinghai, and Tarim Basin of China. The RMB values demonstrate that both datasets underestimated AOD over the Yangtse River Delta and the Central region (MERRA-2 by −0.08 to −0.19, CMIP6 by −0.02 to −0.16) and overestimated AOD (MERRA-2 by 0.01, CMIP6 by 0.60) over the Tarim Basin. However, MERRA-2 underestimated (−0.36) and CMIP6 overestimated AOD (0.17) over Qinghai. Over the Sichuan Basin, both datasets performed poorly due to significant overestimation of lower AOD values, and underestimation of higher ones, which can explain the lower correlations and higher errors.

Seasonally, the evaluation results show that MERRA-2 provides more accurate AOD results at local scales than CMIP6 (Figs. 4 and 5). Specifically, over the Gobi Desert, for MERRA-2 the correlation is higher (r = 0.77) and the error metrics are lower (RMSE = 0.06, MAE = 0.05) in the summer than in the winter, autumn, and spring, whereas for CMIP6 the correlation is highest (r = 0.30) and the error metrics are smaller (RMSE = 0.11, MAE = 0.10) in the summer than in the spring, winter, and autumn. CMIP6 tends to overestimate AOD more than MERRA-2. In addition, in Northeast China, MERRA-2 has a very good correlation (r = 0.91) and lower errors (RMSE = 0.07, MAE = 0.06) in the summer than in the spring, winter, and autumn, while for CMIP6 the highest correlation (r = 0.58) and lowest errors (RMSE = 0.12, MAE = 0.09) occur in the summer, followed by spring, winter and autumn (Figs. 4 and 5). Over the North China Plain, MERRA-2 obtained better AOD results in terms of r (0.86), RMSE (0.09), and MAE (0.07) during the autumn than in the spring, winter, or summer, whereas in comparison the correlation (r = 0.60) and errors (RMSE = 0.42, MAE = 0.38) for the CMIP6 AOD were comparatively higher in the summer than in the spring, winter, or autumn. In the Yangtse River Delta, MERRA-2 AOD compares best with the MODIS DTB AOD during the autumn as indicated by the high correlation (r = 0.81) and the lower error metrics (RMSE = 0.11, and MAE = 0.10), followed by summer, winter, and spring, whereas CMIP6 had inconsistent results. In contrast, across Central China, consistent results between MERRA-2 AOD and MODIS DTB AOD are obtained in the winter (r = 0.82, RMSE = 0.14, MAE = 0.11), followed by summer, autumn, and spring, whereas overall CMIP6 had inconsistent results in all seasons. However, for CMIP6 the correlation is higher and lower errors smaller in the winter (r = 0.61, RMSE = 0.18, MAE = 0.16) than in the autumn, summer, or spring. In the Sichuan Basin, MERRA-2 AOD and MODIS DTB AOD are well correlated in the summer (r = 0.77, RMSE = 0.21, MAE = 0.19), but not in other seasons, while for CMIP6 the AOD is not in good agreement with the MODIS DTB AOD in any season. In addition, both MERRA-2 and CMIP6 significantly overestimate AOD during winter and autumn and underestimates the AOD for the other two seasons (spring and summer), which contributes to the inconsistent results over this area. Like for the North China Plain, the MERRA-2 AOD and MODIS DTB AOD across the Pearl River Delta region compare favorably in the autumn (r = 0.89, RMSE = 0.09, MAE = 0.07) followed by spring, winter, and summer, whereas for CMIP6 the AOD compare reasonably with the MODIS DTB AOD only for the spring (r = 0.79, RMSE = 0.18, MAE = 0.15), rather than winter, autumn, or summer. Over Qinghai, both MERRA-2 AOD and CMIP6 AOD are not in good agreement with the MODIS DTB AOD for all seasons. Notably, CMIP6 overestimates the AOD in autumn and summer and underestimates the AOD in the spring and winter, whereas MERRA-2 significantly underestimates the AOD in all seasons. The Tibetan Plateau is another low AOD area in China, where MERRA-2 AOD is in good agreement with the MODIS DTB AOD in the winter (r = 0.81, RMSE = 0.09, MAE = 0.09) followed by the spring, autumn, and summer, whereas CMIP6 AOD compares well with the MODIS DTB AOD only in the winter (r = 0.79, RMSE = 0.04, MAE = 0.03) and not for the other three seasons. In addition, CMIP6 overestimates the AOD from spring to autumn and underestimates the AOD in the winter, while MERRA-2 underestimates the AOD in all seasons. The Tarim

Basin is the biggest desert in China; here MERRA-2 AOD is in good agreement with the MODIS DTB AOD in the summer (r = 0.82, RMSE = 0.14, MAE = 0.13) followed by the autumn, winter, and spring, whereas CMIP6 AOD did not provide reasonable results in all seasons. In comparison with MERRA-2, CMIP6 significantly overestimated the AOD in the autumn, summer, and winter and underestimates the AOD in the winter. Across all China, MERRA-2 AOD is in good agreement with the MODIS DTB AOD in the autumn (r = 0.86, RMSE = 0.02, MAE = 0.02) followed by summer, winter, and spring, whereas CMIP6 did not perform well in all seasons. CMIP6 significantly overestimates the AOD in the autumn and winter and underestimates in the spring and summer, whereas MERRA-2 underestimates the AOD in all seasons. The underestimation of the AOD by MERRA-2 on both annual and seasonal scales has been reported to probably be due to the uncertainty of the emission inventory used in the GOES models (Buchard et al., 2017; Che et al., 2019b; Shi et al., 2019). In contrast, the significant overestimation of the AOD by CMIP6 probably results from the uncertainty of the Community Emissions Data System (CEDS) inventory adopted by the CMIP6 models (Wang et al., 2021). Overall, MERRA-2 AOD performs better over most regions of China than CMIP6, as concluded from the comparison with MODIS DTB AOD data because of the high correlation and the low error metrics (RMSE and MAE) for MERRA-2.

3.2 Annual and seasonal mean spatial AOD patterns over China

Figure 6 shows the spatial distributions of the annual and seasonal mean AOD, obtained from CMIP6, MERRA-2, and MODIS DTB over China, averaged over the period 2000–2014. Between these three data sets, the annual mean MODIS DTB AOD is highest (> 0.8) over the Central (Henan, Hubei, Hunan), East (Anhui, Jiangsu, Shanghai, Shangdong), North (Tianjin and Hebei), and Southwest (the eastern part of the Sichuan

Basin and the western part of Chongqing) regions of China, whereas the CMIP6 and MERRA-2 over these regions are lower (0.6 – 0.8) (Fig. 6). The second-highest mean MODIS DTB AOD (0.6 – 0.8) is observed over parts of Anhui, Hunan, Jiangxi, Zheijiang, Guandong, Guangxi, and Shanxi. Also in these regions, the CMIP6 and MERRA-2 mean AOD is lower (0.5 – 0.6) than the MODIS DTB AOD. These areas are all low altitude regions (< 500 m above sea level), characterized by high population density and high anthropogenic aerosol emissions owing to rapid urbanization and industrialization (Luo et al., 2014). Besides, Cao et al. (2014) reported that large amounts of coarse particles (soot and dust) were emitted from industrial activities and coal fuel combustion, which constitute a major contribution to the total aerosol loadings over these regions. The high AOD over North China mainly results from the emission of coarse particles (desert dust) from the Taklamakan Desert (Yu et al., 2016; Proestakis et al., 2018). Figure 6 shows that MODIS DTB detected moderate levels of AOD (0.4 – 0.5) over parts of the Northeast (Liaoning, Jilin, Heilongjiang), Fujian, Zheijiang, the Southwest province of Guizhou, the Northwest province of Shanxi, and the Tarim Basin (Xinjiang), with the MERRA-2 AOD close to MODIS DTB AOD and CMIP6 AOD higher than MODIS DTB AOD, especially over the Tarim Basin (Xinjiang). The lowest AOD (< 0.30) was observed by MODIS DTB AOD over high altitude areas with sparse populations such as the North (Inner Mongolia), Northwest (Gansu, Qinghai, Ningxia), and West (Tibetan Plateau) of China. For these regions, MERRA-2 again performed close to MODIS DTB AOD, but CMIP6 overestimated AOD (Fig. 6). Several previous studies also found the lowest AOD over Inner Mongolia, Gansu, Qinghai, Ningxia, and the Tibetan Plateau (Liu et al., 2016; de Leeuw et al., 2018). In conjunction with the above spatial information, seasonally, the MODIS DTB AOD is highest in spring followed by summer, winter, and autumn throughout China, where CMIP6 and MEERA-2 also show similar seasonal scenarios with higher and lower AOD values than MODIS DTB AOD. It is likely that widespread biomass-burning activities, less vegetation, and large amounts of sand and dust lifted from their natural source (the Taklamakan and Gobi Desert) result in high AOD in spring. These results are supported by previously published studies (Luo et al., 2014; He et al., 2016; Liu et al., 2016). As more photochemical reactions occur during the summer, this might be considered as another important possible factor for the second-highest aerosol loadings over the study area (Dickerson et al., 1997). Li and Wang (2014) also documented that the summertime AOD may be influenced by the abundant water vapor and droplets suspended in the atmosphere during the summer season over China.

3.3 Annual and Seasonal mean AOD variability using regional average

Aerosol Optical Depth (AOD) obtained from CMIP6, MERRA-2, and MODIS DTB was averaged from 2000 to 2014 at annual and seasonal scales over the ten major regions selected across China (see Fig.1), for each of the years included in this study (2000–2014). The results are plotted as time series as shown in Figs. 7 and Supplementary Data Figs. S1–S4. The 15-year annual mean high AOD from MODIS DTB was 0.71 ± 0.08 in the North China Plain, where comparatively lower AOD from CMIP6 (0.50 ± 0.04) and MERRA-2 (0.56 ± 0.07) was observed than MODIS DTB (Fig. 7). High AOD values probably result from anthropogenic aerosols produced by industrial and vehicular emissions over these regions, as was also reported by Hu et al. (2018). Due to the nature of the topography and the sparse population, the lower annual mean AOD from MODIS DTB was 0.13 ± 0.01 in the Tibetan Plateau, where CMIP6 (0.16 ± 0.01) and MERRA-2 (0.06 ± 0.005) also show their lowest AOD than MODIS DTB AOD, signifying over- and –underestimation of AOD (Fig. 7 and Table 2).

Seasonal patterns in the AOD were obvious over different regions of China (Supplementary Data Figs. S1–S4 and Table 2). Seasonal mean MODIS DTB AOD was highest in the spring in most regions of China except for North China Plain, where AOD peaked in the summer than other seasons. In the spring, MODIS DTB AOD was highest in Central China (0.81 ± 0.06), where the comparable result was observed from CMIP6 (0.81 ± 0.09) and MERRA-2 underestimates AOD (0.72 ± 0.09) compared to MODIS DTB AOD (Table 2). It is important to mention that MODIS DTB AOD was lowest in the autumn over the North China Plain, Yangtse River Delta, Tarim Basin, Northeast, Gobi Desert, Qinghai as well as Entire China. In the autumn, MODIS DTB AOD was highest in the North China Plain (0.57 ± 0.07), where both CMIP6 (0.48 ± 0.05) and MERRA-2 underestimate AOD (0.50 ± 0.06) than MODIS DTB AOD (Table 2). Several earlier studies also found the highest AOD in the spring and lowest in the autumn (Pan et al., 2010; Deng et al., 2012; Luo et al., 2014; Cheng et al., 2015; Wang et al., 2015; He et al., 2016; De Leeuw et al., 2018). Furthermore, across Central China, the Sichuan Basin, and the Tibetan Plateau of China, MODIS DTB reported low seasonal mean AOD in the winter season. In the winter, MODIS DTB AOD was highest in Central China (0.59 ± 0.08), where both CMIP6 (0.75 ± 0.08) and MERRA-2 underestimate AOD (0.69 ± 0.11) than MODIS DTB AOD (Table 2). Apart from the above-mentioned areas of China, across the Pearl River Delta, MODIS DTB reported low AOD in the summer (0.46 ± 0.08), where both CMIP6 (0.38 ± 0.03) and MERRA-2 underestimate AOD (0.32 ± 0.04) than MODIS DTB AOD (Table 2). Overall, the study concludes that both CMIP6 and MERRA-2 substantially over- and under-estimate AOD across China compared to MODIS DTB AOD, therefore, in section 3.4, the study has calculated AOD trends using MODIS DTB AOD.

3.4 Trends in AOD

Figure 8 shows the spatial distributions of annual and seasonal trends of AOD obtained from MODIS DTB over China for the period 2000 to 2014. It is evident from Fig. 8 and Table 3 that not all regions have statistically significant trends. However, a substantial spatial contrast in AOD trends (both increasing and decreasing) was evident over the study area at annual and seasonal scales (Fig. 8). Annually, decreasing AOD trends from MODIS DTB were evident over the Gobi Desert (−0.004/year) and Qinghai (−0.001/year). Guo et al. (2011) and Li (2020) also found a decreasing AOD trend over the Gobi Desert. In addition, MODIS DTB reported increasing AOD trends from 0.0002/year to 0.014/year across the Northeast, North China plain, Yangtse River Delta, Central, Sichuan Basin, Pearl River Delta, Tarim Basin, and Tibetan Plateau, as well as over Entire China. The increasing AOD trends may be due to the rapid increase in industrial and anthropogenic activities over these regions, resulting in abundant aerosols emitted into the atmosphere; similar results were documented in Zhang et al. (2013) and Gui et al. (2017). Wang et al. (2015) reported that sulfate aerosols from industry were mainly responsible for the increasing AOD trends.

In the winter season, increasing AOD trends from MODIS DTB were observed which varied between 0.0003/year and 0.020/year over most regions of China, except for the Gobi Desert and Tibetan Plateau (Table 3). The increasing AOD trends during the winter may be associated with meteorological conditions in China. Yin et al. (2017) reported that meteorological conditions play a significant role in transporting pollutants and mixing aerosols with local emissions from anthropogenic activities, resulting in an increase in wintertime haze aerosols over China over the last few decades. Wind alone can explain about 10% of the historical rise of regional aerosols (Gu et al., 2018). Liu et al. (2016) documented that different anthropogenic activities linked with biomass and fossil fuel burning were mainly responsible for enhancing AOD levels over Central China, East, and Northeast during the autumn and winter, resulting in increasing AOD trends there. During the spring, MODIS DTB AOD trends were decreasing with values varying from 0.00002/year to 0.009/year over the Gobi Desert, Northeast, Sichuan Basin, Qinghai, as well as across Entire China (Table 3). The decreasing trends indicate a large decrease in coarse-mode aerosol particles generated from natural sources in China. A similar result was reported by Hu et al. (2018). Apart from this, the increasing AOD trends from MODIS DTB from 0.001/year to 0.011/year were observed over the North China Plain, Yangtse River Delta, Central, Pearl River Delta, Tibetan Plateau, and Tarim Basin (Table 3). The increasing AOD trends over South China (Yangtse River Delta) during the spring were attributed to the increased fine-mode particles from large anthropogenic emissions and coarse-mode particles (sea-salt aerosols) from the coast of South China (Dong et al., 2013; Qi et al., 2013; Luo et al., 2014). In the summer, the MODIS DTB AOD trends were decreasing AOD by 0.002–0.007 (per year) over the Gobi Desert, Pearl River Delta, Qinghai, and Tarim Basin (Table 3). Apart from this, the MODIS DTB AOD trends were increasing from 0.0003/year to 0.022/year over the Northeast, North China Plain, Yangtse River Delta, Central, Sichuan Basin, Tibetan Plateau, and Entire China (Table 3). Hu et al. (2018) also found increasing AOD trends over the highly populated and industrialized regions of Central, East, and Northeast of China. The increasing trends reflect the dominance of fine-mode non-absorbing aerosols due to industrial emissions of SO_4 aerosol (Wang et al., 2015). The decreasing AOD trend over the Pearl River Delta was also documented by (Li, 2020). In the autumn, the MODIS DTB AOD trends were increasing and varied from 0.0001/year to 0.010/year over the Northeast, North China Plain, Yangtse

River Delta, Central, Pearl River Delta, Qinghai, Tibetan Plateau, Tarim Basin, and Entire China except for the Gobi Desert and Sichuan Basin, where trends were decreasing with −0.0002 to −0.006 (per year) (Table 3).

In light of the above, AOD increased annually over most regions of China between 2000 and 2014, except for the Gobi Desert and Qinghai, where AOD was found to have reduced. Seasonal deviations in AOD trends were also evident and are different between different parts of China. The SO_2 and primary aerosol emissions increased substantially, relative to dust from 2000 to 2005 due to rapid economic and industrial development, which led to increased AOD (Zhao et al., 2017). The change (increase or decrease) in AOD from 2000 to 2014 can be associated with changes in both meteorology and emissions (Li, 2020). In the next section, we further investigate if there were any co-benefits from China's strict air pollution control policies on AOD during the 11th and 12th Five-Year Plan (FYP) periods. Therefore, we calculated AOD linear trends for 2000–2005, 2006–2010 (11th FYP), and 2011–2014 (12th FYP) (Figs. 9–12).

MODIS DTB AOD trends over China were noticeably decreasing at annual and seasonal scales during the 12th FYP period, following the 11th FYP period and 2000–2005, which was probably due to the implementation of strict air pollution control policies (Figs. 9–11). On the annual scale, MODIS DTB AOD trends were strongly decreasing with −0.003/year to −0.074/year during the 12th FYP period throughout the whole country, except for Northeast, Qinghai, and Tibetan Plateau. These decreasing trends were stronger during the 12th FYP period than during the 11th FYP period and 2000–2005 (Fig. 12). On a seasonal scale, MODIS DTB AOD also strongly decreased during the 12th FYP period across different parts of China as compared to the 11th FYP period and 2000–2005 (Fig. 12). Although China's air pollution control policies during the 11th and 12th FYP periods were not designed for AOD control and prevention, they still had co-benefits as AOD was subsequently found to decrease at both annual and seasonal scales over China.

Several reasons might be considered for the increase and decrease in AOD over the study area. For example, due to rapid economic and industrial development from 2000 to 2005, the emissions of SO_2 and primary aerosols increased substantially relative to dust, resulting in increased AOD over China (Zhao et al., 2017). The reduction of SO_2 and $PM_{2.5}$ (contains: sulfate, nitrate, organic carbon, elemental carbon), and the control of industrial dust with soot (Zhou et al., 2015; Jin et al., 2016; Ma et al., 2019) may have contributed to a decrease in AOD during the 11th FYP period. The effective reduction in anthropogenic emissions could lead to AOD reduction (Sogacheva et al., 2018). The Environmental protection, Energy Conservation and Emissions Reduction (ECER), and Air Pollution Prevention and Control Key Regions (APPC-KR) policies during the 12th FYP period reduced SO_2, NO_x, $PM_{2.5}$, PM_{10}, industrial dust, and soot emissions (Wang et al., 2018), which contributed to decreasing AOD over China. Liu et al. (2021) reported that anthropogenic aerosol species (black carbon, organic carbon, and sulfate) were reduced over the Sichuan Basin because of strict implementation of the air pollution control policies in China during the 12th FYP period, resulting in AOD also reduced in this regions.

4. Conclusion

In the current study, CMIP6 and MERRA-2 AOD were evaluated against MODIS DTB AOD for the years 2000–2014, its long-term spatiotemporal variations were scrutinized and the effectiveness of air pollution control policies to control AOD over China from 2000 to 2014 was considered.

- The evaluation results show higher correlation (r = 0.71–0.89) and lower error (RMSE = 0.07–0.23, MAE = 0.05–0.17) for MERRA-2 than for CMIP6 (r = 0.38–0.66, RMSE = 0.05–0.28, MAE = 0.04–0.23) over the Gobi Desert, Northeast, North China plain, Pearl River Delta, Tibetan Plateau, and Entire China. Likewise, over the Yangtse River Delta, Central, Qinghai, and Tarim Basin, MERRA-2 correlation and error (r = 0.51–0.64, RMSE = 0.11–0.20, MAE = 0.08–0.15) are better than that of CMIP6 (0.06–0.45, 0.13–0.36, 0.09–0.29). Over the Sichuan Basin, poor comparison results were obtained for both MERRA-2 (0.19, 0.23, 0.19) and the CMIP6 (−0.02, 0.24, 0.18). MERRA-2 underestimated AOD, which might result from the uncertainty of the emission inventory used in the Goddard Earth Observing System (GEOS) models. CMIP6 overestimated AOD over most regions, possibly due to the uncertainty of the Community Emissions Data System (CEDS) inventory adopted by CMIP6 models. In any case, it is clear that the CMIP6 and MERRA-2 both need significant improvement in how they simulate AOD.

- During the study period from 2000 to 2014, AOD fromTerra-MODIS DTB was high across the low altitude regions characterized by highly populated, economically, and industrially developed regions of the North China Plain (0.71 ± 0.08) followed by Central China (0.69 ± 0.06), Yangtse River Delta (0.67 ± 0.05), Sichuan Basin (0.64 ± 0.06), and Pearl River Delta (0.54 ± 0.05). AOD levels were lowest over the Tibetan Plateau (0.13 ± 0.01) followed by Qinghai (0.19 ± 0.03) and the Gobi Desert (0.21 ± 0.03), due to the role of topography and sparse population. Seasonally, the highest AOD over China occurred in spring, followed by summer, winter, and autumn. Widespread biomass-burning activities, less vegetation, and the lifting of large amounts of sand and dust particles from natural sources (the Taklamakan and Gobi deserts) may result in high AOD in spring. Moreover, increased photochemical reactivity, and abundant water vapor and droplets in the atmosphere may all contribute to the secondary AOD maximum during the summer.

- AOD trends were shown by Terra-MODIS DTB to be increasing throughout most of the country during 2000–2014 and 2000–2005. Uncontrolled industrialization, urbanization, and strong economic development mostly occurred from 2000 to 2005 in China, which may have led to the overall increasing AOD trends. AOD levels decreased substantially from −0.003/year to −0.074/year, throughout the whole country except for the Northeast, Qinghai, and Tibetan Plateau (here AOD increased by 0.001/year to 0.0.002/year); these trends were greater than during the 11th FYP period. Seasonally, Terra-MODIS DTB AOD showed a prominent decreasing trend in the summer season during the 12th FYP period across different parts of China; stronger than during the 11th FYP period. During the 12th FYP period, strict implementation of China's air pollution control policies may have reduced the anthropogenic emissions of primary aerosols, SO_2, NOx, $PM_{2.5}$ (a combination of sulfate, nitrate, organic carbon, elemental carbon), industrial dust, and soot, which may be possible reasons for the AOD reduction. Evidently, the air pollution control policies had the co-benefit of reducing AOD, resulting in improved air quality over China. Overall, the size of the errors found in CMIP6 and MERRA-2 AOD output suggests that they still cannot be effectively used for air quality monitoring at regional and local scales within a country like China.

CRediT authorship contribution statement

Md. Arfan Ali: Conceptualization, Data curation, Methodology, Formal analysis, Investigation, Validation, Visualization, Writing - original draft. **Muhammad Bilal:** Conceptualization, Supervision, Investigation, Visualization, Writing - review & editing.

Yu Wang: Data curation, Methodology, Formal analysis, Investigation, Validation, Visualization**. Zhongfeng Qiu:** Supervision, Writing - review & editing. **Janet E. Nichol, Gerrit de Leeuw, Alaa Mhawish, Mansour Almazroui, M. Nazrul Islam, Usman Mazhar:** Writing - review & editing. **Birhanu Asmerom Habtemicheal:** Formal analysis & Visualization, **Song Ke:** Data curation.

Acknowledgments

The authors are grateful to NASA for providing satellite and MERRA-2 based aerosol optical depth (AOD). We would like to give special thanks to the Earth Systems and Grid Federation (ESGF) for making CMIP6-based AOD data available. The National Key Research and Development Program of China (2016YFC1400901), Jiangsu Technology Project of Nature Resources (KJXM2019042), the Jiangsu Provincial Department of Education for the Special Project of Jiangsu Distinguished Professor (R2018T22), the National Natural Science Foundation of China (Grant No. 41976165), and the Startup Foundation for Introduction Talent of NUIST (2017r107). The foremost author (Md. Arfan Ali) is highly grateful to the China Scholarship Council (CSC) and NUIST for granting his fellowship and providing the required supports. The study contributes to the ESA / MOST cooperation project DRAGON5, Topic 3 Atmosphere, sub-topic 3.2 Air-Quality.

Supplementary data to this article can be found online at XXXXX

References

Ali, M.A., Assiri, M.E., 2019. Analysis of AOD from MODIS-Merged DT–DB Products Over the Arabian Peninsula. Earth Syst. Environ. 3, 625–636. https://doi.org/10.1007/s41748-019-00108-x.

Ali, M.A., Assiri, M.E., 2016. Spatio-temporal analysis of aerosol concentration over Saudi Arabia using satellite remote sensing techniques. Geogr. Malaysian J. Soc. Sp. 12, 1–11.

Ali, M.A., Assiri, M.E., Dambul, R., 2017. Seasonal Aerosol Optical Depth (AOD) Variability Using Satellite Data and its Comparison over Saudi Arabia for the Period 2002–2013. Aerosol Air Qual. Res. 17, 1267–1280. https://doi.org/10.4209/aaqr.2016.11.0492.

Ali, M.A., Islam, M.M., Islam, M.N., Almazroui, M., 2019. Investigations of MODIS AOD and cloud properties with CERES sensor based net cloud radiative effect and a NOAA HYSPLIT Model over Bangladesh for the period 2001–2016. Atmos. Res. 215, 268–283. https://doi.org/10.1016/j.atmosres.2018.09.001.

Ali, M.A., Nichol, J.E., Bilal, M., Qiu, Z., Mazhar, U., Wahiduzzaman, M., Almazroui, M., Islam, M.N., 2020. Classification of aerosols over Saudi Arabia from 2004–2016. Atmos. Environ. 241, 117785. https://doi.org/10.1016/j.atmosenv.2020.117785.

Almazroui, M., 2019. A comparison study between AOD data from MODIS deep blue collections 51 and 06 and from AERONET over Saudi Arabia. Atmos. Res. 225, 88–95. https://doi.org/10.1016/j.atmosres.2019.03.040.

Bilal, M., Mhawish, A., Nichol, J.E., Qiu, Z., Nazeer, M., Ali, M.A., de Leeuw, G., Levy, R.C., Wang, Y., Chen, Y., Wang, L., Shi, Y., Bleiweiss, M.P., Mazhar, U., Atique, L., Ke, S., 2021a. Air pollution scenario over Pakistan: Characterization and ranking of extremely polluted cities using long-term concentrations of aerosols and trace gases. Remote Sens. Environ. 264, 112617. https://doi.org/10.1016/j.rse.2021.112617.

Bilal, M., Nazeer, M., Nichol, J., Qiu, Z., Wang, L., Bleiweiss, M., Shen, X., Campbell, J., Lolli, S., 2019. Evaluation of Terra-MODIS C6 and C6.1 Aerosol Products against Beijing, XiangHe, and Xinglong AERONET Sites in China during 2004-2014. Remote Sens. 11, 486. https://doi.org/10.3390/rs11050486.

Bilal, M., Nazeer, M., Nichol, J.E., 2017a. Validation of MODIS and VIIRS derived aerosol optical depth over complex coastal waters. Atmos. Res. 186, 43–50. https://doi.org/10.1016/j.atmosres.2016.11.009.

Bilal, M., Nazeer, M., Qiu, Z., Ding, X., Wei, J., 2018. Global Validation of MODIS C6 and C6.1 Merged Aerosol Products over Diverse Vegetated Surfaces. Remote Sens. 10, 475. https://doi.org/10.3390/rs10030475.

Bilal, M., Nichol, J.E., 2017. Evaluation of the NDVI-Based Pixel Selection Criteria of the MODIS C6 Dark Target and Deep Blue Combined Aerosol Product. IEEE J. Sel. Top. Appl. Earth Obs. Remote Sens. 10, 3448–3453. https://doi.org/10.1109/JSTARS.2017.2693289.

Bilal, M., Nichol, J.E., 2015. Evaluation of MODIS aerosol retrieval algorithms over the Beijing-Tianjin-Hebei region during low to very high pollution events. J. Geophys. Res. Atmos. 120, 7941–7957. https://doi.org/10.1002/2015JD023082.

Bilal, M., Nichol, J.E., Nazeer, M., 2016. Validation of Aqua-MODIS C051 and C006 Operational Aerosol Products Using AERONET Measurements Over Pakistan. IEEE J. Sel. Top. Appl. Earth Obs. Remote Sens. 9, 2074–2080. https://doi.org/10.1109/JSTARS.2015.2481460.

Bilal, M., Nichol, J.E., Wang, L., 2017b. New customized methods for improvement of the MODIS C6 Dark Target and Deep Blue merged aerosol product. Remote Sens. Environ. 197, 115–124. https://doi.org/10.1016/j.rse.2017.05.028.

Bilal, M., Qiu, Z., Nichol, J.E., Mhawish, A., Ali, M.A., Khedher, K.M., de Leeuw, G., Yu, W., Tiwari, P., Nazeer, M., Bleiweiss, M.P., 2021b. Uncertainty in Aqua-MODIS Aerosol Retrieval Algorithms During COVID-19 Lockdown. IEEE Geosci. Remote Sens. Lett. 1–5. https://doi.org/10.1109/LGRS.2021.3077189.

Bright, J.M., Gueymard, C.A., 2019. Climate-specific and global validation of MODIS Aqua and Terra aerosol optical depth at 452 AERONET stations. Sol. Energy 183, 594–605. https://doi.org/10.1016/j.solener.2019.03.043.

Buchard, V., Randles, C.A., da Silva, A.M., Darmenov, A., Colarco, P.R., Govindaraju, R., Ferrare, R., Hair, J., Beyersdorf, A.J., Ziemba, L.D., Yu, H., 2017. The MERRA-2 Aerosol Reanalysis, 1980 Onward. Part II: Evaluation and Case Studies. J. Clim. 30, 6851–6872. https://doi.org/10.1175/JCLI-D-16-0613.1.

Butt, M.J., Assiri, M.E., Ali, M.A., 2017. Assessment of AOD variability over Saudi Arabia using MODIS Deep Blue products. Environ. Pollut. 231, 143–153. https://doi.org/10.1016/j.envpol.2017.07.104.

Cao, C., Zheng, S., Singh, R.P., 2014. Characteristics of aerosol optical properties and meteorological parameters during three major dust events (2005–2010) over Beijing, China. Atmos. Res. 150, 129–142. https://doi.org/10.1016/j.atmosres.2014.07.022.

Charlson, R.J., Schwartz, S.E., Hales, J.M., Cess, R.D., Coakley, J.A., Hansen, J.E., Hofmann, D.J., 1992. Climate Forcing by Anthropogenic Aerosols. Science (80-.). 255, 423–430. https://doi.org/10.1126/science.255.5043.423.

Che, H., Gui, K., Xia, X., Wang, Y., Holben, B.N., Goloub, P., Cuevas-Agulló, E., Wang, H., Zheng, Y., Zhao, H., Zhang, X., 2019a. Large contribution of meteorological factors to inter-decadal changes in regional aerosol optical depth. Atmos. Chem. Phys. 19, 10497–10523. https://doi.org/10.5194/acp-19-10497-2019.

Che, H., Yang, L., Liu, C., Xia, X., Wang, Y., Wang, Hong, Wang, Han, Lu, X., Zhang, X., 2019b. Long-term validation of MODIS C6 and C6.1 Dark Target aerosol products over China using CARSNET and AERONET. Chemosphere 236, 124268. https://doi.org/10.1016/j.chemosphere.2019.06.238.

Che, H., Zhang, X.-Y., Xia, X., Goloub, P., Holben, B., Zhao, H., Wang, Y., Zhang, X.-C., Wang, H., Blarel, L., Damiri, B., Zhang, R., Deng, X., Ma, Y., Wang, T., Geng, F., Qi, B., Zhu, J., Yu, J., Chen, Q., Shi, G., 2015a. Ground-based aerosol climatology of China: aerosol optical depths from the China Aerosol Remote Sensing Network (CARSNET) 2002–2013. Atmos. Chem. Phys. 15, 7619–7652. https://doi.org/10.5194/acp-15-7619-2015.

Che, H., Zhang, Xiaoye, Chen, H., Damiri, B., Goloub, P., Li, Z., Zhang, Xiaochun, Wei, Y., Zhou, H., Dong, F., Li, D., Zhou, T., 2009. Instrument calibration and aerosol optical depth validation of the China Aerosol Remote Sensing Network. J. Geophys. Res. 114, D03206. https://doi.org/10.1029/2008JD011030.

Che, H., Zhao, H., Wu, Y., Xia, X., Zhu, J., Dubovik, O., Estelles, V., Ma, Y., Wang, Yangfeng, Wang, H., Wang, Yaqiang, Zhang, X., Shi, G., 2015b. Application of aerosol optical properties to estimate aerosol type from ground-based remote sensing observation at urban area of northeastern China. J. Atmos. Solar-Terrestrial Phys. 132, 37–47. https://doi.org/10.1016/j.jastp.2015.06.015.

Cheng, T., Xu, C., Duan, J., Wang, Y., Leng, C., Tao, J., Che, H., He, Q., Wu, Y., Zhang, R., Li, X., Chen, J., Kong, L., Yu, X., 2015. Seasonal variation and difference of aerosol optical properties in columnar and surface atmospheres over Shanghai. Atmos. Environ. 123, 315–326. https://doi.org/10.1016/j.atmosenv.2015.05.029.

Chu, D.A., Kaufman, Y.J., Ichoku, C., Remer, L.A., Tanré, D., Holben, B.N., 2002. Validation of MODIS aerosol optical depth retrieval over land. Geophys. Res. Lett. 29, 8007. https://doi.org/10.1029/2001GL013205.

de Leeuw, G., Holzer-Popp, T., Bevan, S., Davies, W.H., Descloitres, J., Grainger, R.G., Griesfeller, J., Heckel, A., Kinne, S., Klüser, L., Kolmonen, P., Litvinov, P., Martynenko, D., North, P., Ovigneur, B., Pascal, N., Poulsen, C., Ramon, D., Schulz, M., Siddans, R., Sogacheva, L., Tanré, D., Thomas, G.E., Virtanen, T.H., von Hoyningen Huene, W., Vountas, M., Pinnock, S., 2015. Evaluation of seven European aerosol optical depth retrieval algorithms for climate analysis. Remote Sens. Environ. 162, 295–315. https://doi.org/10.1016/j.rse.2013.04.023.

de Leeuw, G., Sogacheva, L., Rodriguez, E., Kourtidis, K., Georgoulias, A.K., Alexandri, G., Amiridis, V., Proestakis, E., Marinou, E., Xue, Y., van der A, R., 2018. Two decades of satellite observations of AOD over mainland China using ATSR-2, AATSR and MODIS/Terra: data set evaluation and large-scale patterns. Atmos. Chem. Phys. 18, 1573–1592. https://doi.org/10.5194/acp-18-1573-2018.

de Meij, A., Pozzer, A., Lelieveld, J., 2012. Trend analysis in aerosol optical depths and pollutant emission estimates between 2000 and 2009. Atmos. Environ. 51, 75–85. https://doi.org/10.1016/j.atmosenv.2012.01.059.

Deng, X., Shi, C., Wu, B., Chen, Z., Nie, S., He, D., Zhang, H., 2012. Analysis of aerosol characteristics and their relationships with meteorological parameters over Anhui province in China. Atmos. Res. 109–110, 52–63. https://doi.org/10.1016/j.atmosres.2012.02.011.

Dickerson, R.R., Kondragunta, S., Stenchikov, G., Civerolo, K.L., Doddridge, B.G., Holben, B.N., 1997. The Impact of Aerosols on Solar Ultraviolet Radiation and Photochemical Smog. Science 278(5339), 827–830. https://doi.org/10.1126/science.278.5339.827.

Dong, Z., Yu, X., Li, X., Dai, J., 2013. Analysis of variation trends and causes of aerosol optical depth in Shaanxi Province using MODIS data. Chinese Sci. Bull. 58, 4486–4496. https://doi.org/10.1007/s11434-013-5991-z.

Eyring, V., Bony, S., Meehl, G.A., Senior, C.A., Stevens, B., Stouffer, R.J., Taylor, K.E., 2016. Overview of the Coupled Model Intercomparison Project Phase 6 (CMIP6) experimental design and organization. Geosci. Model Dev. 9, 1937–1958. https://doi.org/10.5194/gmd-9-1937-2016.

Filonchyk, M., Hurynovich, V., 2020. Validation of MODIS Aerosol Products with AERONET Measurements of Different Land Cover Types in Areas over Eastern Europe and China. J. Geovisualization Spat. Anal. 4, 10. https://doi.org/10.1007/s41651-020-00052-9.

Filonchyk, M., Yan, H., Zhang, Z., Yang, S., Li, W., Li, Y., 2019. Combined use of satellite and surface observations to study aerosol optical depth in different regions of China. Sci. Rep. 9, 6174. https://doi.org/10.1038/s41598-019-42466-6.

Flemming, J., Benedetti, A., Inness, A., Engelen, R.J., Jones, L., Huijnen, V., Remy, S., Parrington, M., Suttie, M., Bozzo, A., Peuch, V.-H., Akritidis, D., Katragkou, E., 2017. The CAMS interim Reanalysis of Carbon Monoxide, Ozone and Aerosol for 2003–2015. Atmos. Chem. Phys. 17, 1945–1983. https://doi.org/10.5194/acp-17-1945-2017.

Gelaro, R., McCarty, W., Suárez, M.J., Todling, R., Molod, A., Takacs, L., Randles, C.A., Darmenov, A., Bosilovich, M.G., Reichle, R., Wargan, K., Coy, L., Cullather, R., Draper, C., Akella, S., Buchard, V., Conaty, A., da Silva, A.M., Gu, W., Kim, G.-K., Koster, R., Lucchesi, R., Merkova, D., Nielsen, J.E., Partyka, G., Pawson, S., Putman, W., Rienecker, M., Schubert, S.D., Sienkiewicz, M., Zhao, B., 2017. The Modern-Era Retrospective Analysis for Research and Applications, Version 2 (MERRA-2). J. Clim. 30, 5419–5454. https://doi.org/10.1175/JCLI-D-16-0758.1.

Georgoulias, A.K., Alexandri, G., Kourtidis, K.A., Lelieveld, J., Zanis, P., Amiridis, V., 2016. Differences between the MODIS Collection 6 and 5.1 aerosol datasets over the greater Mediterranean region. Atmos. Environ. 147, 310–319. https://doi.org/10.1016/j.atmosenv.2016.10.014.

Gu, X., Bao, F., Cheng, T., Chen, H., Wang, Y., Guo, H., 2018. The impacts of regional transport and meteorological factors on aerosol optical depth over Beijing, 1980–2014. Sci. Rep. 8, 5113. https://doi.org/10.1038/s41598-018-22803-x.

Gui, K., Che, H., Chen, Q., Zeng, Z., Zheng, Y., Long, Q., Sun, T., Liu, X., Wang, Y., Liao, T., Yu, J., Wang, H., Zhang, X., 2017. Water vapor variation and the effect of aerosols in China. Atmos. Environ. 165, 322–335. https://doi.org/10.1016/j.atmosenv.2017.07.005.

Guo, J.-P., Zhang, X.-Y., Wu, Y.-R., Zhaxi, Y., Che, H.-Z., La, B., Wang, W., Li, X.-W., 2011. Spatio-temporal variation trends of satellite-based aerosol optical depth in China during 1980–2008. Atmos. Environ. 45, 6802–6811. https://doi.org/10.1016/j.atmosenv.2011.03.068.

Hauser, A., 2005. NOAA AVHRR derived aerosol optical depth over land. J. Geophys. Res. 110, D08204. https://doi.org/10.1029/2004JD005439.

He, Q., Zhang, M., Huang, B., 2016. Spatio-temporal variation and impact factors analysis of satellite-based aerosol optical depth over China from 2002 to 2015. Atmos. Environ. 129, 79–90. https://doi.org/10.1016/j.atmosenv.2016.01.002.

Holben, B.N., Eck, T.F., Slutsker, I., Tanré, D., Buis, J.P., Setzer, A., Vermote, E., Reagan, J.A., Kaufman, Y.J., Nakajima, T., Lavenu, F., Jankowiak, I., Smirnov, A., 1998. AERONET—A Federated Instrument Network and Data Archive for Aerosol Characterization. Remote Sens. Environ. 66, 1–16. https://doi.org/10.1016/S0034-4257(98)00031-5.

Holben, B.N., Tanré, D., Smirnov, A., Eck, T.F., Slutsker, I., Abuhassan, N., Newcomb, W.W., Schafer, J.S., Chatenet, B., Lavenu, F., Kaufman, Y.J., Castle, J. Vande, Setzer, A., Markham, B., Clark, D., Frouin, R., Halthore, R., Karneli, A., O’Neill, N.T., Pietras, C., Pinker, R.T., Voss, K., Zibordi, G., 2001. An emerging ground-based aerosol climatology: Aerosol optical depth from AERONET. J. Geophys. Res. Atmos. 106, 12067–12097. https://doi.org/10.1029/2001JD900014.

Holzer-Popp, T., de Leeuw, G., Griesfeller, J., Martynenko, D., Klüser, L., Bevan, S., Davies, W., Ducos, F., Deuzé, J.L., Graigner, R.G., Heckel, A., von Hoyningen-Hüne, W., Kolmonen, P., Litvinov, P., North, P., Poulsen, C.A., Ramon, D., Siddans, R., Sogacheva, L., Tanre, D., Thomas, G.E., Vountas, M., Descloitres, J., Griesfeller, J., Kinne, S., Schulz, M., Pinnock, S., 2013. Aerosol retrieval experiments in the ESA Aerosol_cci project. Atmos. Meas. Tech. 6, 1919–1957. https://doi.org/10.5194/amt-6-1919-2013.

Hsu, N.C., Jeong, M.-J., Bettenhausen, C., Sayer, A.M., Hansell, R., Seftor, C.S., Huang, J., Tsay, S.-C., 2013. Enhanced Deep Blue aerosol retrieval algorithm: The second generation. J. Geophys. Res. Atmos. 118, 9296–9315. https://doi.org/10.1002/jgrd.50712.

Hsu, N.C., Tsay, S.-C., King, M.D., Herman, J.R., 2006. Deep Blue Retrievals of Asian Aerosol Properties During ACE-Asia. IEEE Trans. Geosci. Remote Sens. 44, 3180–3195. https://doi.org/10.1109/TGRS.2006.879540.

Hu, K., Kumar, K.R., Kang, N., Boiyo, R., Wu, J., 2018. Spatiotemporal characteristics of aerosols and their trends over mainland China with the recent Collection 6 MODIS and OMI satellite datasets. Environ. Sci. Pollut. Res. 25, 6909–6927. https://doi.org/10.1007/s11356-017-0715-6.

Huang, G., Chen, Y., Li, Z., Liu, Q., Wang, Y., He, Q., Liu, T., Liu, X., Zhang, Y., Gao, J., Yao, Y., 2020. Validation and Accuracy Analysis of the Collection 6.1 <scp>MODIS</scp> Aerosol Optical Depth Over the Westernmost City in China Based on the Sun-Sky Radiometer Observations From SONET. Earth Sp. Sci. 7. https://doi.org/10.1029/2019EA001041.

Huang, Y., Zhu, B., Zhu, Z., Zhang, T., Gong, W., Ji, Y., Xia, X., Wang, L., Zhou, X., Chen, D., 2019. Evaluation and Comparison of MODIS Collection 6.1 and Collection 6 Dark Target Aerosol Optical Depth over Mainland China Under Various Conditions Including Spatiotemporal Distribution, Haze Effects, and Underlying Surface. Earth Sp. Sci. 6, 2575–2592. https://doi.org/10.1029/2019EA000809.

IPCC, 2013. Climate Change 2013: The Physical Science Basis. Contribution of Working Group I to the Fifth Assessment Report of the Intergovernmental Panel on Climate Change, in: Stocker, T.F., D. Qin, G.-K. Plattner, M. Tignor, S.K. Allen, J. Boschung, A. Nauels, Y. Xia, V.B. and P.M.M. (Ed.), IPCC. Cambridge University Press, Cambridge, United Kingdom and New York, NY, USA, p. 1535.

Islam, M.N., Ali, M.A., Islam, M.M., 2019. Spatiotemporal Investigations of Aerosol Optical Properties Over Bangladesh for the Period 2002–2016. Earth Syst. Environ. 3, 563–573. https://doi.org/10.1007/s41748-019-00120-1.

Jin, Y., Andersson, H., Zhang, S., 2016. Air Pollution Control Policies in China: A Retrospective and Prospects. Int. J. Environ. Res. Public Health 13, 1219. https://doi.org/10.3390/ijerph13121219.

Kahn, R.A., Gaitley, B.J., Garay, M.J., Diner, D.J., Eck, T.F., Smirnov, A., Holben, B.N., 2010. Multiangle Imaging SpectroRadiometer global aerosol product assessment by comparison with the Aerosol Robotic Network. J. Geophys. Res. 115, D23209. https://doi.org/10.1029/2010JD014601.

Kang, N., Kumar, K.R., Hu, K., Yu, X., Yin, Y., 2016a. Long-term (2002–2014) evolution and trend in Collection 5.1 Level-2 aerosol products derived from the MODIS and MISR sensors over the Chinese Yangtze River Delta. Atmos. Res. 181, 29–43. https://doi.org/10.1016/j.atmosres.2016.06.008.

Kang, N., Kumar, K.R., Yu, X., Yin, Y., 2016b. Column-integrated aerosol optical properties and direct radiative forcing over the urban-industrial megacity Nanjing in the Yangtze River Delta, China. Environ. Sci. Pollut. Res. 23, 17532–17552. https://doi.org/10.1007/s11356-016-6953-1.

Kaufman, Y.J., Tanré, D., Remer, L.A., Vermote, E.F., Chu, A., Holben, B.N., 1997. Operational remote sensing of tropospheric aerosol over land from EOS moderate resolution imaging spectroradiometer. J. Geophys. Res. Atmos. 102, 17051–17067. https://doi.org/10.1029/96JD03988.

Kong, L., Xin, J., Zhang, W., Wang, Y., 2016. The empirical correlations between PM2.5, PM10 and AOD in the Beijing metropolitan region and the PM2.5, PM10 distributions retrieved by MODIS. Environ. Pollut. 216, 350–360. https://doi.org/10.1016/j.envpol.2016.05.085.

Levy, R.C., Mattoo, S., Munchak, L.A., Remer, L.A., Sayer, A.M., Patadia, F., Hsu, N.C., 2013. The Collection 6 MODIS aerosol products over land and ocean. Atmos. Meas. Tech. 6, 2989–3034. https://doi.org/10.5194/amt-6-2989-2013.

Levy, R.C., Munchak, L.A., Mattoo, S., Patadia, F., Remer, L.A., Holz, R.E., 2015. Towards a long-term global aerosol optical depth record: applying a consistent aerosol retrieval algorithm to MODIS and VIIRS-observed reflectance. Atmos. Meas. Tech. 8, 4083–4110. https://doi.org/10.5194/amt-8-4083-2015.

Levy, R.C., Remer, L.A., Kleidman, R.G., Mattoo, S., Ichoku, C., Kahn, R., Eck, T.F., 2010. Global evaluation of the Collection 5 MODIS dark-target aerosol products over land. Atmos. Chem. Phys. 10, 10399–10420. https://doi.org/10.5194/acp-10-10399-2010.

Li, J., 2020. Pollution Trends in China from 2000 to 2017: A Multi-Sensor View from Space. Remote Sens. 12, 208. https://doi.org/10.3390/rs12020208.

Li, L., Wang, Y., 2015. What drives the aerosol distribution in Guangdong - the most developed province in Southern China? Sci. Rep. 4, 5972. https://doi.org/10.1038/srep05972.

Li, R., Ma, X., Xiong, F., Jia, H., Sha, T., Tian, R., 2020. Comparisons and evaluation of aerosol burden and optical depth in CMIP5 simulations over East Asia. J. Atmos. Solar-Terrestrial Phys. 206, 105315. https://doi.org/10.1016/j.jastp.2020.105315.

Li, Y., Shi, G., Sun, Z., 2020. Evaluation and improvement of MODIS aerosol optical depth products over China. Atmos. Environ. 223, 117251. https://doi.org/10.1016/j.atmosenv.2019.117251.

Li, Z.Q., Xu, H., Li, K.T., Li, D.H., Xie, Y.S., Li, L., Zhang, Y., Gu, X.F., Zhao, W., Tian, Q.J., Deng, R.R., Su, X.L., Huang, B., Qiao, Y.L., Cui, W.Y., Hu, Y., Gong, C.L., Wang, Y.Q., Wang, X.F., Wang, J.P., Du, W.B., Pan, Z.Q., Li, Z.Z., Bu, D., 2018. Comprehensive Study of Optical, Physical, Chemical, and Radiative Properties of Total Columnar Atmospheric Aerosols over China: An Overview of Sun–Sky Radiometer Observation Network (SONET) Measurements. Bull. Am. Meteorol. Soc. 99, 739–755. https://doi.org/10.1175/BAMS-D-17-0133.1.

Liu, H., Remer, L.A., Huang, J., Huang, H.-C., Kondragunta, S., Laszlo, I., Oo, M., Jackson, J.M., 2014. Preliminary evaluation of S-NPP VIIRS aerosol optical thickness. J. Geophys. Res. Atmos. 119, 3942–3962. https://doi.org/10.1002/2013JD020360.

Liu, H., Yan, R., Yang, J., 2021. Credibility and statistical characteristics of CAMSRA and MERRA-2 AOD reanalysis products over the Sichuan Basin during 2003–2018. Atmos. Environ. 244, 117980. https://doi.org/10.1016/j.atmosenv.2020.117980.

Liu, X., Chen, Q., Che, H., Zhang, R., Gui, K., Zhang, H., Zhao, T., 2016. Spatial distribution and temporal variation of aerosol optical depth in the Sichuan basin, China, the recent ten years. Atmos. Environ. 147, 434–445. https://doi.org/10.1016/j.atmosenv.2016.10.008.

Luo, Y., Zheng, X., Zhao, T., Chen, J., 2014. A climatology of aerosol optical depth over China from recent 10 years of MODIS remote sensing data. Int. J. Climatol. 34, 863–870. https://doi.org/10.1002/joc.3728.

Ma, X., Wang, J., Yu, F., Jia, H., Hu, Y., 2016. Can MODIS AOD be employed to derive PM2.5 in Beijing-Tianjin-Hebei over China? Atmos. Res. 181, 250–256. https://doi.org/10.1016/j.atmosres.2016.06.018.

Mei, L., Zhao, C., de Leeuw, G., Che, H., Che, Y., Rozanov, V., Vountas, M., Burrows, J.P., 2019. Understanding MODIS dark-target collection 5 and 6 aerosol data over China: Effect of surface type, aerosol loading and aerosol absorption. Atmos. Res. 228, 161–175. https://doi.org/10.1016/j.atmosres.2019.05.023.

Mhawish, A., Banerjee, T., Broday, D.M., Misra, A., Tripathi, S.N., 2017. Evaluation of MODIS Collection 6 aerosol retrieval algorithms over Indo-Gangetic Plain: Implications of aerosols types and mass loading. Remote Sens. Environ. 201, 297–313. https://doi.org/10.1016/j.rse.2017.09.016.

Misra, A., Kanawade, V.P., Tripathi, S.N., 2016. Quantitative assessment of AOD from 17 CMIP5 models based on satellite-derived AOD over India. Ann. Geophys. 34, 657–671. https://doi.org/10.5194/angeo-34-657-2016.

Molod, A., Takacs, L., Suarez, M., Bacmeister, J., 2015. Development of the GEOS-5 atmospheric general circulation model: evolution from MERRA to MERRA2. Geosci. Model Dev. 8, 1339–1356. https://doi.org/10.5194/gmd-8-1339-2015.

Mortier, A., Gliß, J., Schulz, M., Aas, W., Andrews, E., Bian, H., Chin, M., Ginoux, P., Hand, J., Holben, B., Zhang, H., Kipling, Z., Kirkevåg, A., Laj, P., Lurton, T., Myhre, G., Neubauer, D., Olivié, D., von Salzen, K., Skeie, R.B., Takemura, T., Tilmes, S., 2020. Evaluation of climate model aerosol trends with ground-based observations over the last 2 decades – an AeroCom and CMIP6 analysis. Atmos. Chem. Phys. 20, 13355–13378. https://doi.org/10.5194/acp-20-13355-2020.

Nichol, J., Bilal, M., 2016. Validation of MODIS 3 km Resolution Aerosol Optical Depth Retrievals Over Asia. Remote Sens. 8, 328. https://doi.org/10.3390/rs8040328.

Nichol, J.E., Bilal, M., Ali, M.A., Qiu, Z., 2020. Air Pollution Scenario over China during COVID-19. Remote Sens. 12, 2100. https://doi.org/10.3390/rs12132100.

Pan, L., Che, H., Geng, F., Xia, X., Wang, Y., Zhu, C., Chen, M., Gao, W., Guo, J., 2010. Aerosol optical properties based on ground measurements over the Chinese Yangtze Delta Region. Atmos. Environ. 44, 2587–2596. https://doi.org/10.1016/j.atmosenv.2010.04.013.

Popp, T., de Leeuw, G., Bingen, C., Brühl, C., Capelle, V., Chedin, A., Clarisse, L., Dubovik, O., Grainger, R., Griesfeller, J., Heckel, A., Kinne, S., Klüser, L., Kosmale, M., Kolmonen, P., Lelli, L., Litvinov, P., Mei, L., North, P., Pinnock, S., Povey, A., Robert, C., Schulz, M., Sogacheva, L., Stebel, K., Stein Zweers, D., Thomas, G., Tilstra, L., Vandenbussche, S., Veefkind, P., Vountas, M., Xue, Y., 2016. Development, Production and Evaluation of Aerosol Climate Data Records from European Satellite Observations (Aerosol_cci). Remote Sens. 8, 421. https://doi.org/10.3390/rs8050421.

Proestakis, E., Amiridis, V., Marinou, E., Georgoulias, A.K., Solomos, S., Kazadzis, S., Chimot, J., Che, H., Alexandri, G., Binietoglou, I., Daskalopoulou, V., Kourtidis, K.A., de Leeuw, G., van der A, R.J., 2018. Nine-year spatial and temporal evolution of desert dust aerosols over South and East Asia as revealed by CALIOP. Atmos. Chem. Phys. 18, 1337–1362. https://doi.org/10.5194/acp-18-1337-2018.

Qi, Y., Ge, J., Huang, J., 2013. Spatial and temporal distribution of MODIS and MISR aerosol optical depth over northern China and comparison with AERONET. Chinese Sci. Bull. 58, 2497–2506. https://doi.org/10.1007/s11434-013-5678-5.

Qiu, Z., Ali, M.A., Nichol, J.E., Bilal, M., Tiwari, P., Habtemicheal, B.A., Almazroui, M., Mondal, S.K., Mazhar, U., Wang, Y., Sarker, S., Mustafa, F., Rahman, M.A., 2021. Spatiotemporal Investigations of Multi-Sensor Air Pollution Data over Bangladesh during COVID-19 Lockdown. Remote Sens. 13, 877. https://doi.org/10.3390/rs13050877.

Randles, C.A., da Silva, A.M., Buchard, V., Colarco, P.R., Darmenov, A., Govindaraju, R., Smirnov, A., Holben, B., Ferrare, R., Hair, J., Shinozuka, Y., Flynn, C.J., 2017. The MERRA-2 Aerosol Reanalysis, 1980 Onward. Part I: System Description and Data Assimilation Evaluation. J. Clim. 30, 6823–6850. https://doi.org/10.1175/JCLI-D-16-0609.1.

Remer, L.A., Kaufman, Y.J., Tanré, D., Mattoo, S., Chu, D.A., Martins, J. V., Li, R.-R., Ichoku, C., Levy, R.C., Kleidman, R.G., Eck, T.F., Vermote, E., Holben, B.N., 2005. The MODIS Aerosol Algorithm, Products, and Validation. J. Atmos. Sci. 62, 947–973. https://doi.org/10.1175/JAS3385.1.

Remer, L.A., Mattoo, S., Levy, R.C., Munchak, L.A., 2013. MODIS 3 km aerosol product: algorithm and global perspective. Atmos. Meas. Tech. 6, 1829–1844. https://doi.org/10.5194/amt-6-1829-2013.

Rienecker, M.M., Suarez, M.J., Gelaro, R., Todling, R., Bacmeister, J., Liu, E., Bosilovich, M.G., Schubert, S.D., Takacs, L., Kim, G.-K., Bloom, S., Chen, J., Collins, D., Conaty, A., da Silva, A., Gu, W., Joiner, J., Koster, R.D., Lucchesi, R., Molod, A., Owens, T., Pawson, S., Pegion, P., Redder, C.R., Reichle, R., Robertson, F.R., Ruddick, A.G., Sienkiewicz, M., Woollen, J., 2011. MERRA: NASA's Modern-Era Retrospective Analysis for Research and Applications. J. Clim. 24, 3624–3648. https://doi.org/10.1175/JCLI-D-11-00015.1.

Sayer, A.M., Hsu, N.C., Bettenhausen, C., Jeong, M.-J., Holben, B.N., Zhang, J., 2012. Global and regional evaluation of over-land spectral aerosol optical depth retrievals from SeaWiFS. Atmos. Meas. Tech. 5, 1761–1778. https://doi.org/10.5194/amt-5-1761-2012.

Sayer, A.M., Hsu, N.C., Bettenhausen, C., Jeong, M. -J., Meister, G., 2015. Effect of MODIS Terra radiometric calibration improvements on Collection 6 Deep Blue aerosol products: Validation and Terra/Aqua consistency. J. Geophys. Res. Atmos. 120. https://doi.org/10.1002/2015JD023878.

Sayer, A.M., Hsu, N.C., Lee, J., Kim, W. V., Dutcher, S.T., 2019. Validation, Stability, and Consistency of MODIS Collection 6.1 and VIIRS Version 1 Deep Blue Aerosol Data

Over Land. J. Geophys. Res. Atmos. 124, 4658–4688. https://doi.org/10.1029/2018JD029598.

Sayer, A.M., Munchak, L.A., Hsu, N.C., Levy, R.C., Bettenhausen, C., Jeong, M.-J., 2014. MODIS Collection 6 aerosol products: Comparison between Aqua's e-Deep Blue, Dark Target, and "merged" data sets, and usage recommendations. J. Geophys. Res. Atmos. 119, 13,965-13,989. https://doi.org/10.1002/2014JD022453.

Shao, P., Xin, J., An, J., Kong, L., Wang, B., Wang, J., Wang, Y., Wu, D., 2017. The empirical relationship between PM2.5 and AOD in Nanjing of the Yangtze River Delta. Atmos. Pollut. Res. 8, 233–243. https://doi.org/10.1016/j.apr.2016.09.001.

Shi, H., Xiao, Z., Zhan, X., Ma, H., Tian, X., 2019. Evaluation of MODIS and two reanalysis aerosol optical depth products over AERONET sites. Atmos. Res. 220, 75–80. https://doi.org/10.1016/j.atmosres.2019.01.009.

Sockol, A., Small Griswold, J.D., 2017. Intercomparison between CMIP5 model and MODIS satellite-retrieved data of aerosol optical depth, cloud fraction, and cloud-aerosol interactions. Earth Sp. Sci. 4, 485–505. https://doi.org/10.1002/2017EA000288.

Sogacheva, L., de Leeuw, G., Rodriguez, E., Kolmonen, P., Georgoulias, A.K., Alexandri, G., Kourtidis, K., Proestakis, E., Marinou, E., Amiridis, V., Xue, Y., van der A, R.J., 2018. Spatial and seasonal variations of aerosols over China from two decades of multi-satellite observations – Part 1: ATSR (1995–2011) and MODIS C6.1 (2000–2017). Atmos. Chem. Phys. 18, 11389–11407. https://doi.org/10.5194/acp-18-11389-2018.

Sogacheva, L., Popp, T., Sayer, A.M., Dubovik, O., Garay, M.J., Heckel, A., Hsu, N.C., Jethva, H., Kahn, R.A., Kolmonen, P., Kosmale, M., de Leeuw, G., Levy, R.C., Litvinov, P., Lyapustin, A., North, P., Torres, O., Arola, A., 2020. Merging regional and global aerosol optical depth records from major available satellite products. Atmos. Chem. Phys. 20, 2031–2056. https://doi.org/10.5194/acp-20-2031-2020.

Song, R., Yang, L., Liu, M., Li, C., Yang, Y., 2019. Spatiotemporal Distribution of Air Pollution Characteristics in Jiangsu Province, China. Adv. Meteorol. 2019, 1–14. https://doi.org/10.1155/2019/5907673.

Su, B., Wu, D., Zhang, M., Bilal, M., Li, Y., Li, B.-L., Atique, L., Zhang, Z., Howari, F.M., 2021. Spatio-Temporal Characteristics of PM2.5, PM10, and AOD over the Central Line Project of China's South-North Water Diversion in Henan Province (China). Atmosphere (Basel). 12, 225. https://doi.org/10.3390/atmos12020225.

Sun, E., Xu, X., Che, H., Tang, Z., Gui, K., An, L., Lu, C., Shi, G., 2019. Variation in MERRA-2 aerosol optical depth and absorption aerosol optical depth over China from 1980 to 2017. J. Atmos. Solar-Terrestrial Phys. 186, 8–19. https://doi.org/10.1016/j.jastp.2019.01.019.

Tan, C., Zhao, T., Xu, X., Liu, J., Zhang, L., Tang, L., 2015. Climatic analysis of satellite aerosol data on variations of submicron aerosols over East China. Atmos. Environ. 123, 392–398. https://doi.org/10.1016/j.atmosenv.2015.03.054.

Tian, X., Gao, Z., 2019. Validation and Accuracy Assessment of MODIS C6.1 Aerosol Products over the Heavy Aerosol Loading Area. Atmosphere (Basel). 10, 548. https://doi.org/10.3390/atmos10090548.

Torres, O., Bhartia, P.K., Herman, J.R., Sinyuk, A., Ginoux, P., Holben, B., 2002. A Long-Term Record of Aerosol Optical Depth from TOMS Observations and Comparison to AERONET Measurements. J. Atmos. Sci. 59, 398–413. https://doi.org/10.1175/1520-0469(2002)059<0398:ALTROA>2.0.CO;2.

Torres, O., Tanskanen, A., Veihelmann, B., Ahn, C., Braak, R., Bhartia, P.K., Veefkind, P., Levelt, P., 2007. Aerosols and surface UV products from Ozone Monitoring Instrument observations: An overview. J. Geophys. Res. 112, D24S47. https://doi.org/10.1029/2007JD008809.

Wang, L., Gong, W., Xia, X., Zhu, J., Li, J., Zhu, Z., 2015. Long-term observations of aerosol optical properties at Wuhan, an urban site in Central China. Atmos. Environ. 101, 94–102. https://doi.org/10.1016/j.atmosenv.2014.11.021.

Wang, L., Li, P., Yu, S., Mehmood, K., Li, Z., Chang, S., Liu, W., Rosenfeld, D., Flagan, R.C., Seinfeld, J.H., 2018. Predicted impact of thermal power generation emission control measures in the Beijing-Tianjin-Hebei region on air pollution over Beijing, China. Sci. Rep. 8, 934. https://doi.org/10.1038/s41598-018-19481-0.

Wang, Q., Sun, L., Wei, J., Yang, Y., Li, R., Liu, Q., Chen, L., 2017. Validation and Accuracy Analysis of Global MODIS Aerosol Products over Land. Atmosphere (Basel). 8, 155. https://doi.org/10.3390/atmos8080155.

Wang, Y., Ali, M.A., Bilal, M., Qiu, Z., Ke, S., Almazroui, M., Islam, M.M., Zhang, Y., 2021. Identification of Aerosol Pollution Hotspots in Jiangsu Province of China. Remote Sens. 13, 2842. https://doi.org/10.3390/rs13142842.

Wang, Y., Yuan, Q., Li, T., Shen, H., Zheng, L., Zhang, L., 2019. Evaluation and comparison of MODIS Collection 6.1 aerosol optical depth against AERONET over regions in China with multifarious underlying surfaces. Atmos. Environ. 200, 280–301. https://doi.org/10.1016/j.atmosenv.2018.12.023.

Wang, Z., Lin, L., Xu, Y., Che, H., Zhang, X., Zhang, H., Dong, W., Wang, C., Gui, K., Xie, B., 2021. Incorrect Asian aerosols affecting the attribution and projection of regional climate change in CMIP6 models. npj Clim. Atmos. Sci. 4, 2. https://doi.org/10.1038/s41612-020-00159-2.

Wei, J., Li, Z., Sun, L., Peng, Y., Liu, L., He, L., Qin, W., Cribb, M., 2020. MODIS Collection 6.1 3 km resolution aerosol optical depth product: global evaluation and uncertainty analysis. Atmos. Environ. 240, 117768. https://doi.org/10.1016/j.atmosenv.2020.117768.

Wilks, D.S., 2007. Statistical methods in the atmospheric sciences, second edition, Meteorological Applications.

Xia, X., Che, H., Shi, H., Chen, H., Zhang, X., Wang, P., Goloub, P., Holben, B., 2021. Advances in sunphotometer-measured aerosol optical properties and related topics in China: Impetus and perspectives. Atmos. Res. 249, 105286. https://doi.org/10.1016/j.atmosres.2020.105286.

Xia, X.A., Chen, H.B., Wang, P.C., Zhang, W.X., Goloub, P., Chatenet, B., Eck, T.F., Holben, B.N., 2006. Variation of column-integrated aerosol properties in a Chinese urban region. J. Geophys. Res. 111, D05204. https://doi.org/10.1029/2005JD006203.

Xin, J., Gong, C., Liu, Z., Cong, Z., Gao, W., Song, T., Pan, Y., Sun, Y., Ji, D., Wang, L., Tang, G., Wang, Y., 2016. The observation-based relationships between PM 2.5 and AOD over China. J. Geophys. Res. Atmos. 121, 10701-10716. https://doi.org/10.1002/2015JD024655.

Xin, J., Wang, Yuesi, Pan, Y., Ji, D., Liu, Z., Wen, T., Wang, Yinghong, Li, X., Sun, Y., Sun, J., Wang, P., Wang, G., Wang, X., Cong, Z., Song, T., Hu, B., Wang, Lili, Tang, G., Gao, W., Guo, Y., Miao, H., Tian, S., Wang, Lu, 2015. The Campaign on Atmospheric Aerosol Research Network of China: CARE-China. Bull. Am. Meteorol. Soc. 96, 1137–1155. https://doi.org/10.1175/BAMS-D-14-00039.1.

Yang, J., Hu, M., 2018. Filling the missing data gaps of daily MODIS AOD using spatiotemporal interpolation. Sci. Total Environ. 633, 677–683. https://doi.org/10.1016/j.scitotenv.2018.03.202.

Yin, Z., Wang, H., Chen, H., 2017. Understanding severe winter haze events in the North China Plain in 2014: roles of climate anomalies. Atmos. Chem. Phys. 17, 1641–1651. https://doi.org/10.5194/acp-17-1641-2017.

You, W., Zang, Z., Pan, X., Zhang, L., Chen, D., 2015. Estimating PM2.5 in Xi'an, China using aerosol optical depth: A comparison between the MODIS and MISR retrieval models. Sci. Total Environ. 505, 1156–1165. https://doi.org/10.1016/j.scitotenv.2014.11.024.

Yousefi, R., Wang, F., Ge, Q., Shaheen, A., 2020. Long-term aerosol optical depth trend over Iran and identification of dominant aerosol types. Sci. Total Environ. 722, 137906. https://doi.org/10.1016/j.scitotenv.2020.137906.

Yu, X., Lü, R., Kumar, K.R., Ma, J., Zhang, Q., Jiang, Y., Kang, N., Yang, S., Wang, J., Li, M., 2016. Dust aerosol properties and radiative forcing observed in spring during 2001–2014 over urban Beijing, China. Environ. Sci. Pollut. Res. 23, 15432–15442. https://doi.org/10.1007/s11356-016-6727-9.

Yu, X., Zhu, B., Zhang, M., 2009. Seasonal variability of aerosol optical properties over Beijing. Atmos. Environ. 43, 4095–4101. https://doi.org/10.1016/j.atmosenv.2009.03.061.

Zhang, Q., Tie, X., Lin, W., Cao, J., Quan, J., Ran, L., Xu, W., 2013. Variability of SO_2 in an intensive fog in North China Plain: Evidence of high solubility of SO_2. Particuology 11, 41–47. https://doi.org/10.1016/j.partic.2012.09.005.

Zhang, X. Y., Wang, Y.Q., Niu, T., Zhang, X.C., Gong, S.L., Zhang, Y.M., Sun, J.Y., 2012. Atmospheric aerosol compositions in China: spatial/temporal variability, chemical signature, regional haze distribution and comparisons with global aerosols. Atmos. Chem. Phys. 12, 779–799. https://doi.org/10.5194/acp-12-779-2012.

Zhang, Z., Zhang, M., Bilal, M., Su, B., Zhang, C., Guo, L., 2020. Comparison of MODIS- and CALIPSO-Derived Temporal Aerosol Optical Depth over Yellow River Basin (China) from 2007 to 2015. Earth Syst. Environ. 4, 535–550. https://doi.org/10.1007/s41748-020-00181-7.

Zhao, B., Jiang, J.H., Gu, Y., Diner, D., Worden, J., Liou, K.-N., Su, H., Xing, J., Garay, M., Huang, L., 2017. Decadal-scale trends in regional aerosol particle properties and their linkage to emission changes. Environ. Res. Lett. 12, 054021. https://doi.org/10.1088/1748-9326/aa6cb2

Zhao, T.X.P., Laszlo, I., Guo, W., Heidinger, A., Cao, C., Jelenak, A., Tarpley, D., Sullivan, J., 2008. Study of long-term trend in aerosol optical thickness observed from operational AVHRR satellite instrument. J. Geophys. Res. 113, D07201. https://doi.org/10.1029/2007JD009061.

Zhou, K., Yang, S., Shen, C., Ding, S., Sun, C., 2015. Energy conservation and emission reduction of China's electric power industry. Renew. Sustain. Energy Rev. 45, 10–19. https://doi.org/10.1016/j.rser.2015.01.056.

List of Figures

Fig. 5. Seasonal evaluation of MERRA-2 AOD with respect to MODIS DTB AOD over different areas of China from 2000–2014. The normalized data density is shown in color. The black dash line = 1:1 and red solid line = regression line.

Fig. 6. Annual and seasonal mean spatial distribution of AOD obtained from CMIP6, MERRA-2, and MODIS DTB over China during 2000–2014.

Fig. 7. Annual variabilities in AOD acquired from CMIP6, MERRA-2, and MODIS DTB for major areas of China during the years 2000–2014.

Fig. 8. Annual and seasonal spatial trends in AOD were obtained from MODIS DTB over China for the period 2000–2014.

Fig. 9. Annual and seasonal spatial trends in AOD were obtained from the MODIS DTB AOD data over China for the period 2000–2005.

Fig. 10. Annual and seasonal spatial trends in AOD were obtained from the MODIS DTB AOD data over China for the period 2006–2010.

Fig. 11. Annual and seasonal spatial trends in AOD were obtained from the MODIS DTB AOD data over China for the period 2011–2014.

Fig. 12. Annually and seasonally AOD trends were obtained from MODIS DTB AOD data over China for the period 2000–2005, 11th FYP (2006–2010), and 12th FYP (2011–2014).

<u>List of Tables</u>

Table 3 Trends in AOD derived from the MODIS DTB AOD data over major areas of China for the period 2000–2014. The asterisk (*) indicates significance at 95% confidence level.

Supplementary Data

Fig. S1. Variabilities in wintertime AOD acquired from CMIP6, MERRA-2, and MODIS DTB for major areas of China during the years 2000–2014.

Fig. S2. Variabilities in springtime AOD acquired from CMIP6, MERRA-2, and MODIS DTB for major areas of China during the years 2000–2014.

Fig. S3. Variabilities in summertime AOD acquired from CMIP6, MERRA-2, and MODIS DTB for major areas of China during the years 2000–2014.

Fig. S4. Variabilities in autumn AOD acquired from CMIP6, MERRA-2, and MODIS DTB for major areas of China during the years 2000–2014.

Table 1 Summary of the 15 CMIP6 models used in the study.

S.L.	Models	Modelling Country	Variant Label	Spatial Resolution (°)
1	AWI-ESM-1-1-LR	Germany	r1i1p1f1	0.9×0.9
2	BCC-ESM1	China	r1i1p1f1	1.125×1.125
3	CanESM5	Canada	r1i1p1f1	2.8×2.8
4	CESM2	USA	r1i1p1f1	0.9×1.3
5	CESM2-FV2	USA	r1i1p1f1	2.5×1.9
6	CESM2-WACCM	USA	r1i1p1f1	1.3×0.9
7	CESM2-WACCM-FV2	USA	r1i1p1f1	2.5×1.9
8	CMCC-CM2-SR5	Italy	r1i1p1f1	1.0×1.0
9	E3SM-1-0	USA	r1i1p1f1	1.0×1.0
10	GISS-E2-1-G	USA	r1i1p5f1	2.0×2.5
11	HadGEM3-GC31-LL	UK	r1i1p1f3	1.25×1.85
12	MPI_ESM_1_2_HAM	Germany	r1i1p1f1	1.875×1.875
13	MPI_ESM1_2_HR	Germany	r5i1p1f1	1.0×1.0
14	NorESM2-LM	Norway	r1i1p1f1	2.0×2.0
15	UKESM1-0-LL	UK	r1i1p1f1	1.9×1.3

Table 2 Mean annual and seasonal AOD obtained from CMIP6 Ensemble, MERRA-2 reanalysis, and Terra-MODIS over major areas of China for the period 2000–2014.

Areas	AOD	Winter	Spring	Summer	Autumn	Annual
Gobi Desert	CMIP6	0.22±0.02	0.40±0.02	0.33±0.02	0.33±0.02	0.32±0.01
	MERRA-2	0.16±0.02	0.29±0.03	0.28±0.03	0.19±0.02	0.23±0.01
	MODIS DTB	0.15±0.02	0.31±0.06	0.24±0.05	0.13±0.02	0.21±0.03
Northeast	CMIP6	0.20±0.01	0.34±0.05	0.35±0.03	0.27±0.02	0.29±0.02
	MERRA-2	0.16±0.03	0.39±0.11	0.38±0.08	0.23±0.04	0.29±0.09
	MODIS DTB	0.24±0.06	0.42±0.11	0.34±0.08	0.23±0.06	0.31±0.08
North China Plain	CMIP6	0.40±0.04	0.55±0.04	0.58±0.05	0.48±0.05	0.50±0.04
	MERRA-2	0.41±0.07	0.58±0.09	0.73±0.11	0.50±0.06	0.56±0.07
	MODIS DTB	0.60±0.11	0.72±0.09	0.96±0.17	0.57±0.07	0.71±0.08
Yangtse River Delta	CMIP6	0.55±0.05	0.66±0.06	0.51±0.05	0.52±0.04	0.56±0.05
	MERRA-2	0.55±0.09	0.63±0.06	0.52±0.08	0.47±0.08	0.54±0.07
	MODIS DTB	0.61±0.07	0.77±0.05	0.74±0.10	0.56±0.06	0.67±0.05
Central	CMIP6	0.75±0.08	0.81±0.09	0.54±0.06	0.64±0.06	0.68±0.07
	MERRA-2	0.69±0.11	0.72±0.09	0.52±0.08	0.62±0.10	0.64±0.09
	MODIS DTB	0.59±0.08	0.81±0.06	0.73±0.12	0.64±0.09	0.69±0.06
Sichuan Basin	CMIP6	0.70±0.07	0.71±0.08	0.51±0.06	0.66±0.09	0.65±0.08
	MERRA-2	0.74±0.12	0.71±0.10	0.48±0.07	0.63±0.10	0.64±0.09
	MODIS DTB	0.48±0.17	0.80±0.07	0.67±0.08	0.60±0.08	0.64±0.06
Pearl River Delta	CMIP6	0.50±0.04	0.58±0.06	0.38±0.03	0.46±0.04	0.48±0.04
	MERRA-2	0.49±0.08	0.64±0.12	0.32±0.04	0.46±0.09	0.48±0.07
	MODIS DTB	0.48±0.07	0.71±0.07	0.46±0.08	0.52±0.09	0.54±0.05
Qinghai	CMIP6	0.14±0.01	0.24±0.01	0.23±0.02	0.25±0.03	0.22±0.01
	MERRA-2	0.06±0.01	0.18±0.01	0.14±0.051	0.08±0.01	0.12±0.01
	MODIS DTB	0.16±0.03	0.31±0.06	0.16±0.06	0.12±0.02	0.19±0.03
Tibetan Plateau	CMIP6	0.12±0.01	0.16±0.01	0.18±0.02	0.15±0.02	0.16±0.01
	MERRA-2	0.03±0.004	0.10±0.01	0.08±0.01	0.04±0.005	0.06±0.005
	MODIS DTB	0.09±0.01	0.20±0.02	0.13±0.02	0.10±0.01	0.13±0.01
Tarim Basin	CMIP6	0.31±0.04	0.68±0.04	0.69±0.06	0.68±0.03	0.59±0.03
	MERRA-2	0.21±0.03	0.47±0.04	0.48±0.05	0.34±0.05	0.37±0.02
	MODIS DTB	0.20±0.05	0.73±0.12	0.36±0.06	0.19±0.05	0.37±0.04
Entire China	CMIP6	0.30±0.03	0.43±0.03	0.38±0.02	0.38±0.03	0.37±0.02
	MERRA-2	0.24±0.03	0.37±0.04	0.32±0.03	0.26±0.03	0.30±0.03
	MODIS DTB	0.31±0.03	0.47±0.04	0.40±0.04	0.27±0.02	0.36±0.02

Table 3 Trends in AOD derived from the MODIS DTB AOD data over major areas of China from 2000–2014. The asterisk (*) indicates significance at 95% confidence level.

Areas	Winter	Spring	Summer	Autumn	Annual
Gobi Desert	-0.002	-0.006	-0.007*	-0.0002	-0.004*
Northeast	0.008*	-0.009	0.007	0.008*	0.003
North China Plain	0.020*	0.005	0.022*	0.010*	0.014*
Yangtse River Delta	0.012*	0.001	0.008	0.005	0.006*
Central China	0.014*	0.003	0.011	0.005	0.008*
Sichuan Basin	0.008	-0.0003	0.006	-0.006	0.001
Pearl River Delta	0.003	0.011*	-0.002	0.0001	0.003
Qinghai	0.0003	-0.00002	-0.005	0.001	-0.001
Tibetan Plateau	-0.0002	0.001	0.0003	0.0002	0.0002
Tarim Basin	0.0004	0.003	-0.004	0.006*	0.001
Entire China	0.002	-0.0003	0.002	0.003*	0.002

Declaration of interests

☒ The authors declare that they have no known competing financial interests or personal relationships that could have appeared to influence the work reported in this paper.

☐The authors declare the following financial interests/personal relationships which may be considered as potential competing interests:

1208 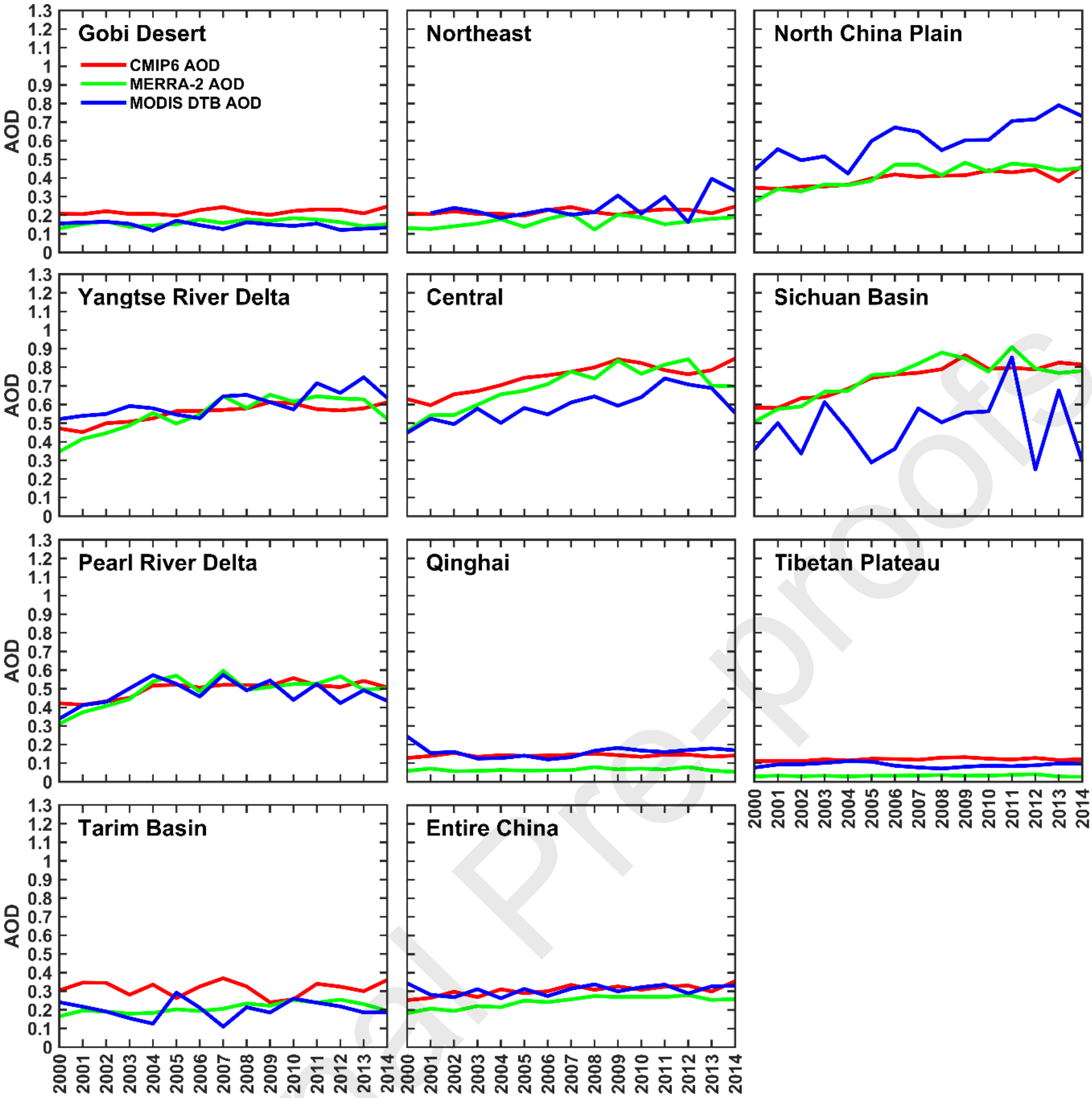
Gobi Desert
CMIP6 AOD
MERRA-2 AOD
MODIS DTB AOD
Northeast
North China Plain
Yangtse River Delta
Central
Sichuan Basin
Pearl River Delta
Qinghai
Tibetan Plateau
Tarim Basin
Entire China
AOD

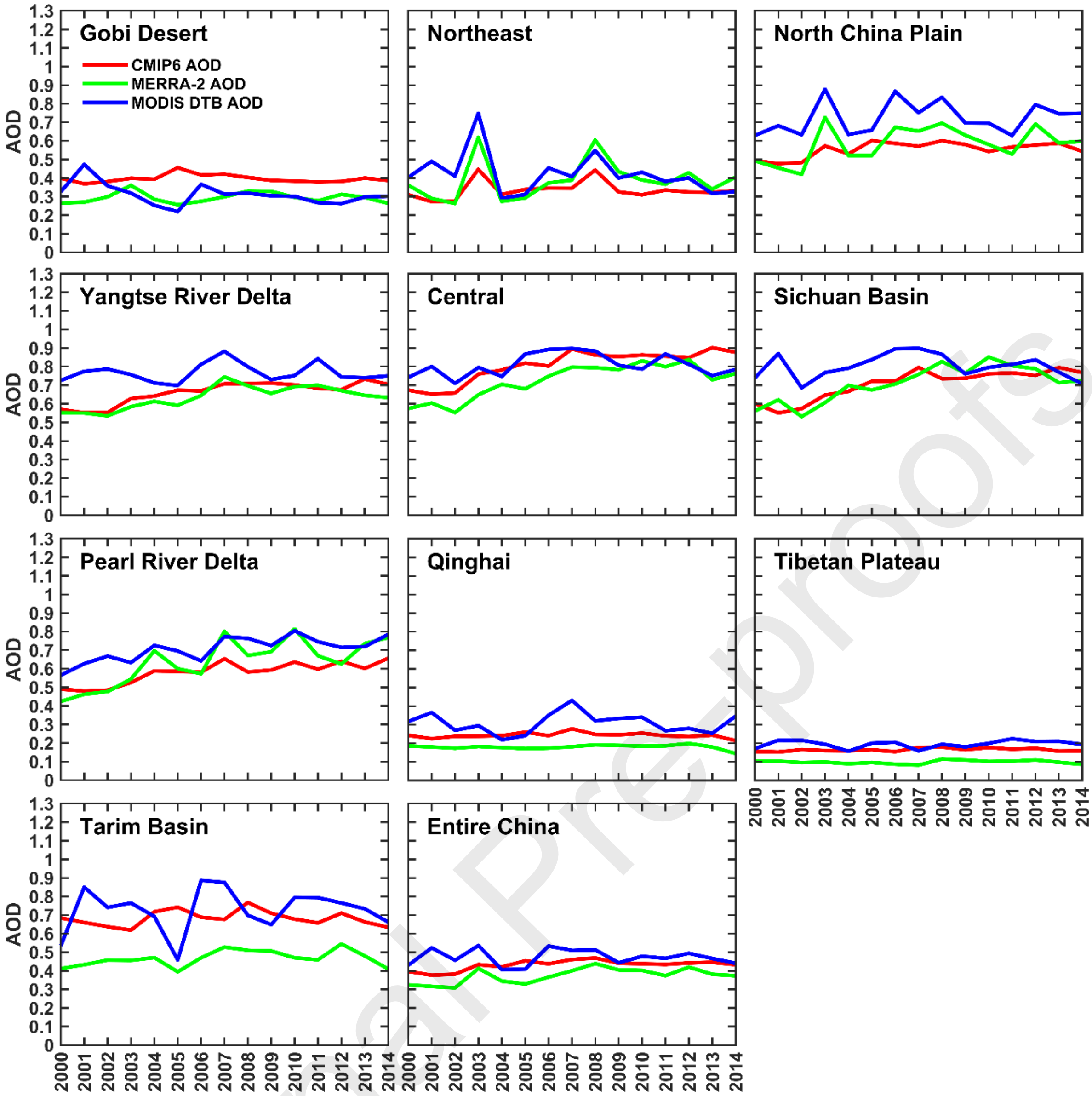
Gobi Desert
Northeast
North China Plain
Yangtse River Delta
Central
Sichuan Basin
Pearl River Delta
Qinghai
Tibetan Plateau
Tarim Basin
Entire China
CMIP6 AOD
MERRA-2 AOD
MODIS DTB AOD
AOD

1209

1210 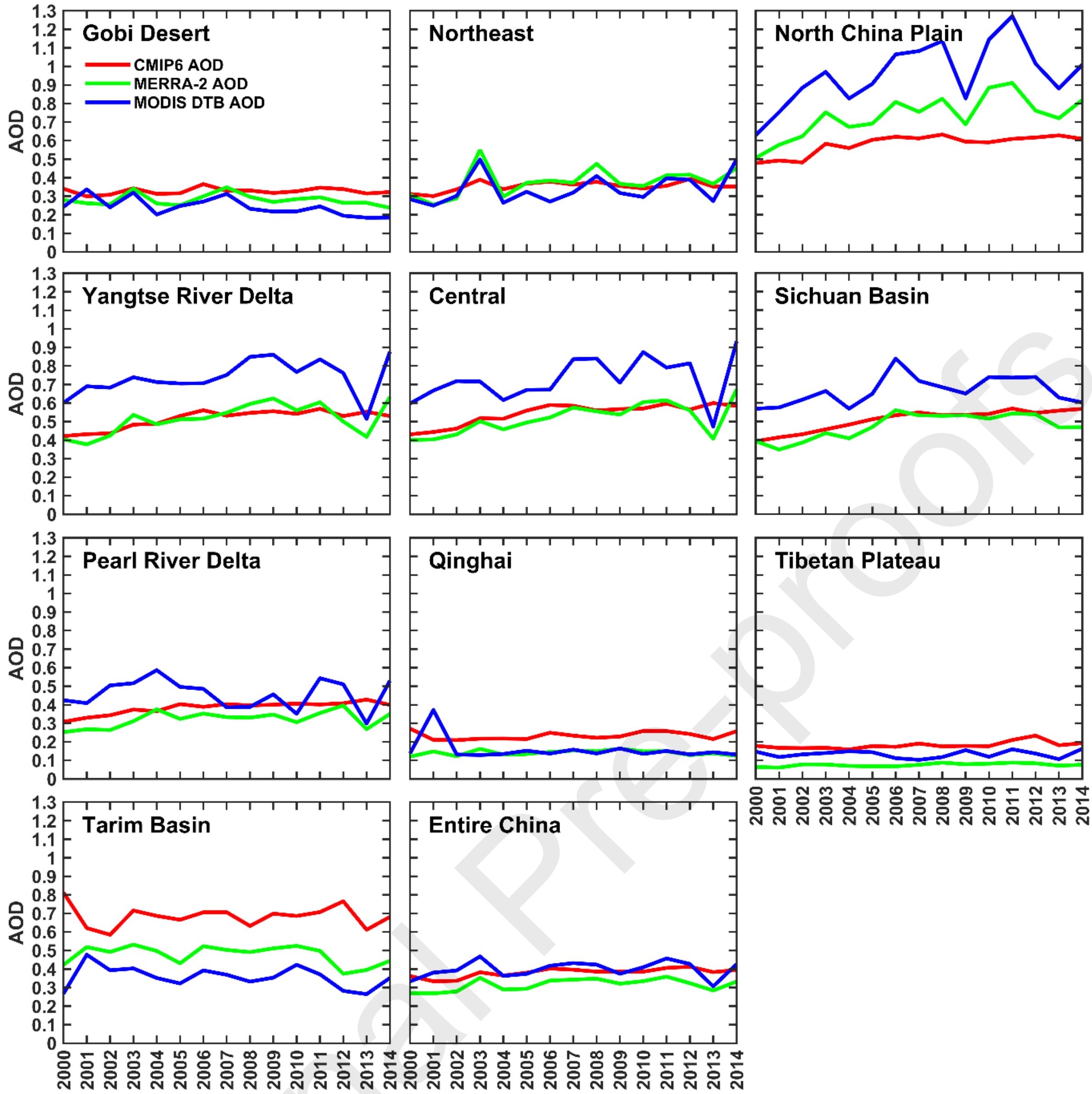
Gobi Desert
CMIP6 AOD
MERRA-2 AOD
MODIS DTB AOD
Northeast
North China Plain
Yangtse River Delta
Central
Sichuan Basin
Pearl River Delta
Qinghai
Tibetan Plateau
Tarim Basin
Entire China
AOD

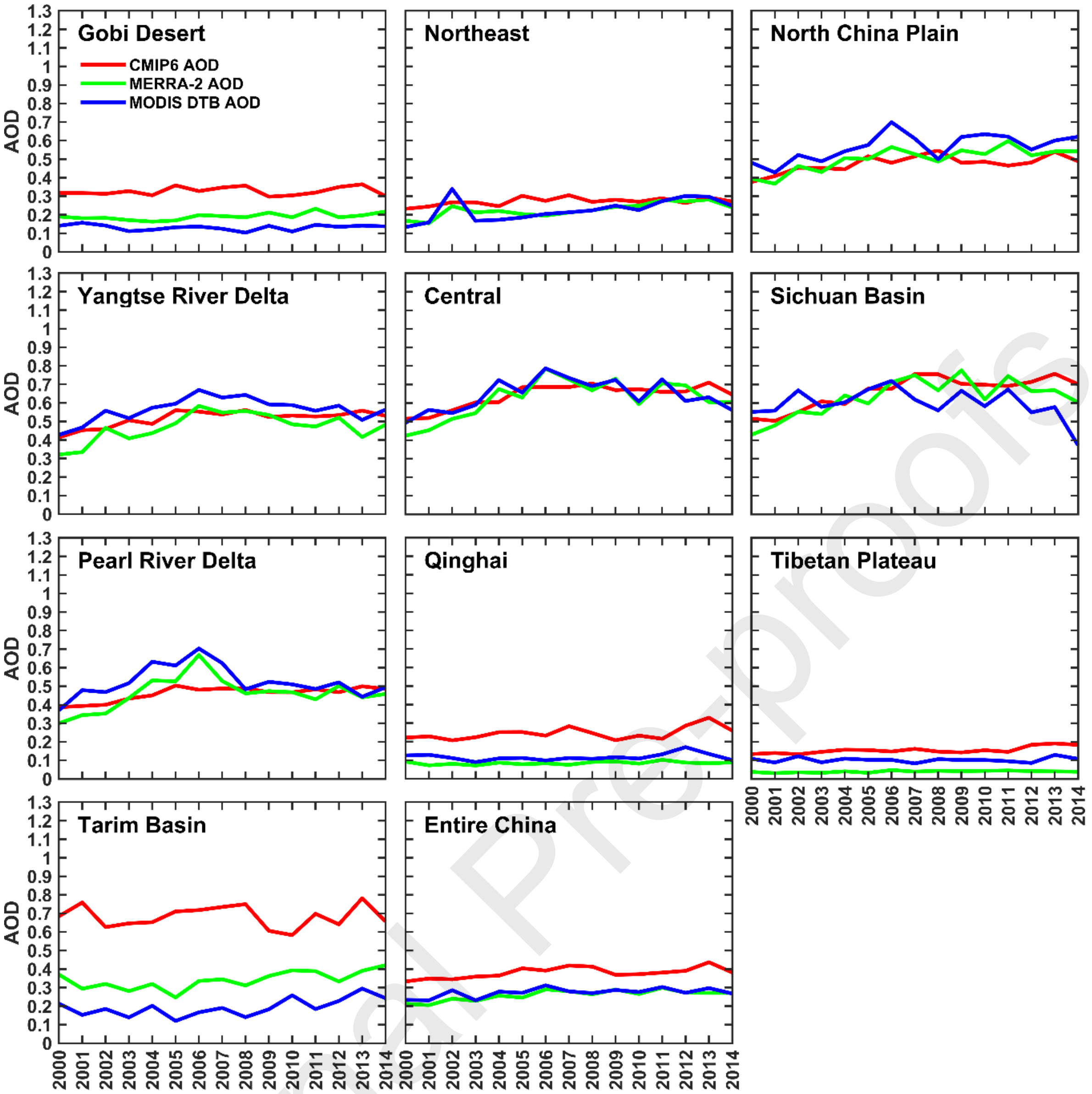
Gobi Desert
CMIP6 AOD
MERRA-2 AOD
MODIS DTB AOD
Northeast
North China Plain
Yangtse River Delta
Central
Sichuan Basin
Pearl River Delta
Qinghai
Tibetan Plateau
Tarim Basin
Entire China
AOD
2000 2001 2002 2003 2004 2005 2006 2007 2008 2009 2010 2011 2012 2013 2014

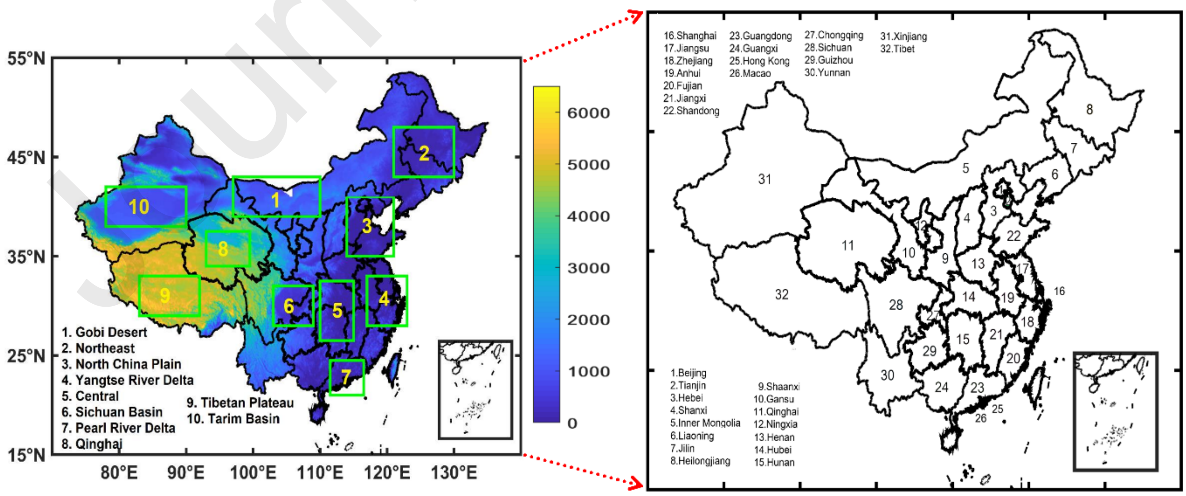
1. Gobi Desert
2. Northeast
3. North China Plain
4. Yangtse River Delta
5. Central
6. Sichuan Basin
7. Pearl River Delta
8. Qinghai
9. Tibetan Plateau
10. Tarim Basin
55°N 45°N 35°N 25°N 15°N
80°E 90°E 100°E 110°E 120°E 130°E
6000 5000 4000 3000 2000 1000 0
1.Beijing
2.Tianjin
3.Hebei
4.Shanxi
5.Inner Mongolia
6.Liaoning
7.Jilin
8.Heilongjiang
9.Shaanxi
10.Gansu
11.Qinghai
12.Ningxia
13.Henan
14.Hubei
15.Hunan
16.Shanghai
17.Jiangsu
18.Zhejiang
19.Anhui
20.Fujian
21.Jiangxi
22.Shandong
23.Guangdong
24.Guangxi
25.Hong Kong
26.Macao
27.Chongqing
28.Sichuan
29.Guizhou
30.Yunnan
31.Xinjiang
32.Tibet

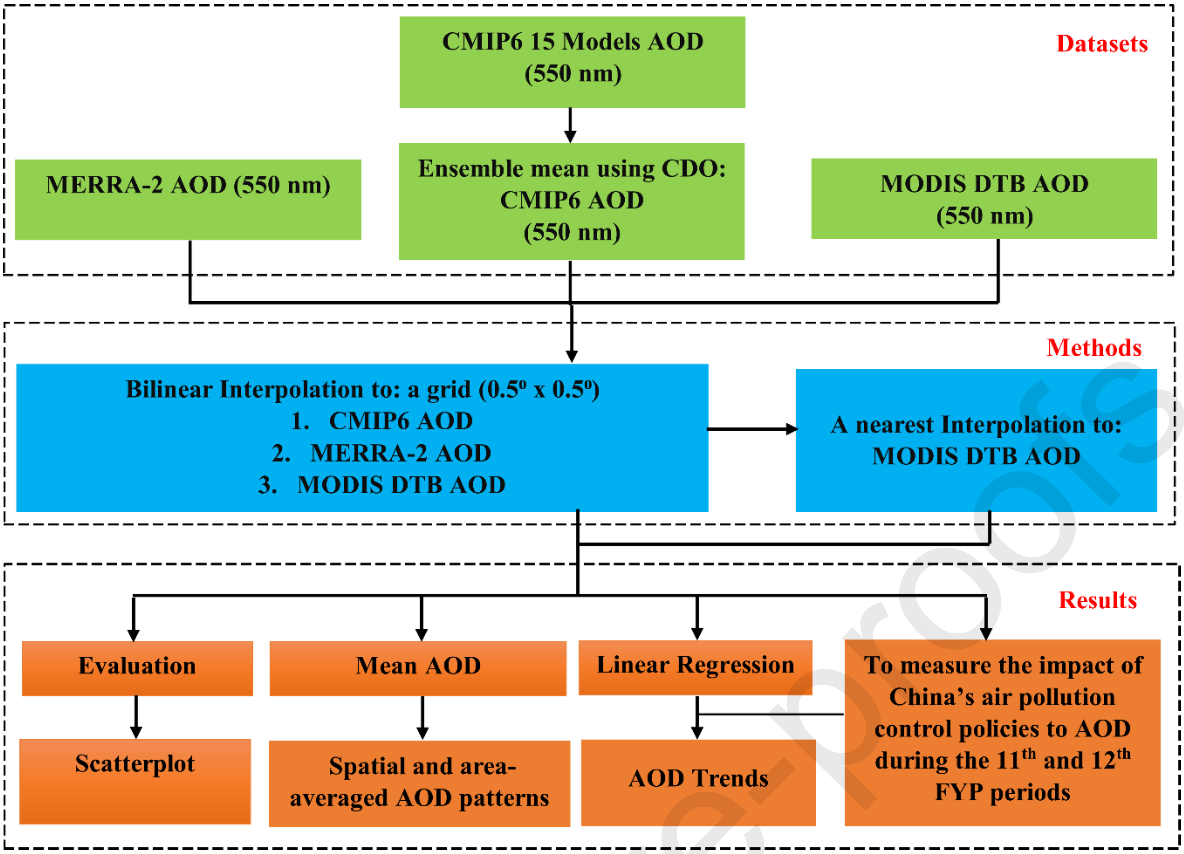
CMIP6 15 Models AOD (550 nm)
Datasets
MERRA-2 AOD (550 nm)
Ensemble mean using CDO: CMIP6 AOD (550 nm)
MODIS DTB AOD (550 nm)
Methods
Bilinear Interpolation to: a grid (0.5° x 0.5°)
1. CMIP6 AOD
2. MERRA-2 AOD
3. MODIS DTB AOD
A nearest Interpolation to: MODIS DTB AOD
Results
Evaluation
Mean AOD
Linear Regression
To measure the impact of China's air pollution control policies to AOD during the 11th and 12th FYP periods
Scatterplot
Spatial and area-averaged AOD patterns
AOD Trends

1213

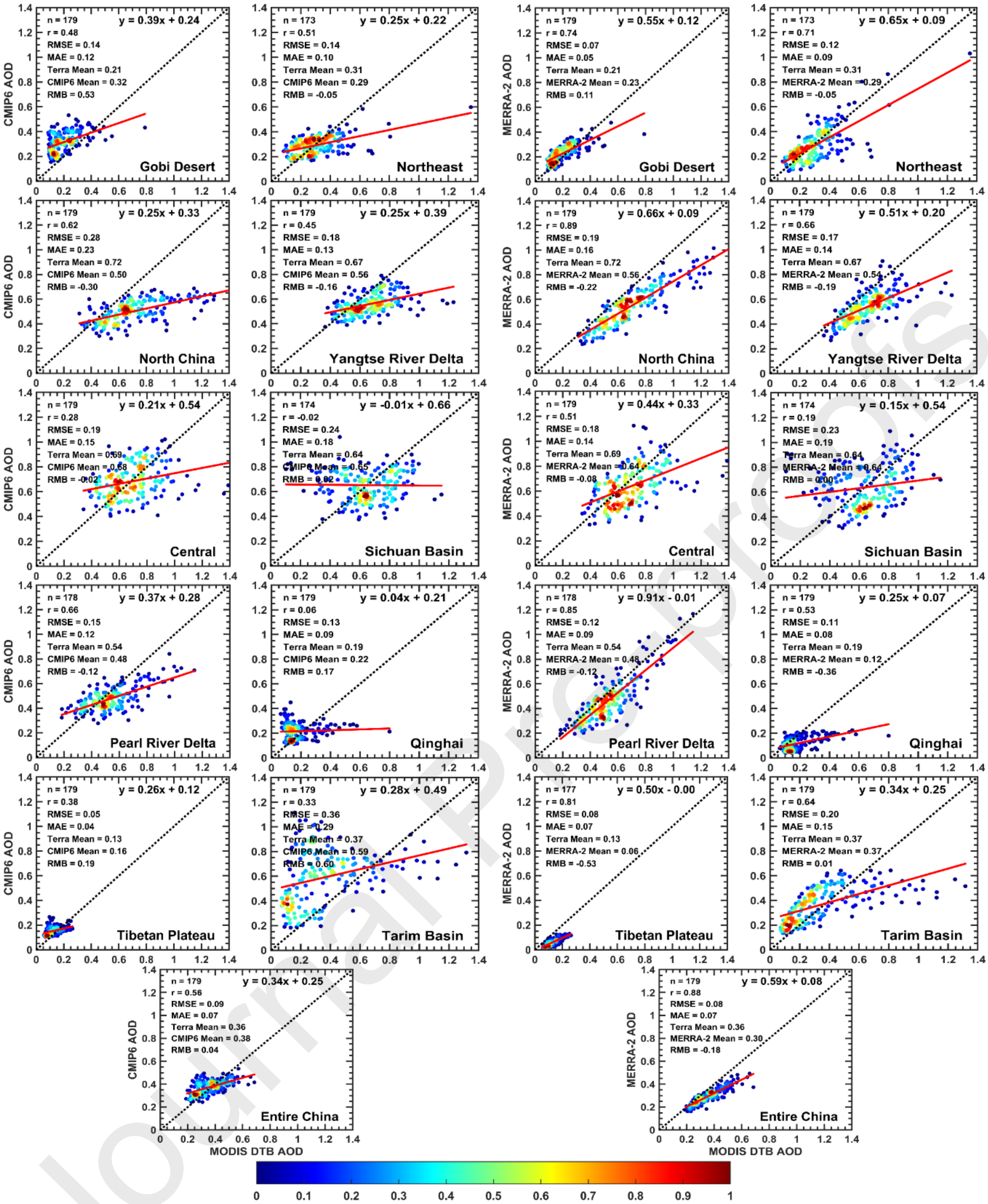
n = 179
y = 0.39x + 0.24
r = 0.48
RMSE = 0.14
MAE = 0.12
Terra Mean = 0.21
CMIP6 Mean = 0.32
RMB = 0.53
Gobi Desert
n = 173
y = 0.25x + 0.22
r = 0.51
RMSE = 0.14
MAE = 0.10
Terra Mean = 0.31
CMIP6 Mean = 0.29
RMB = -0.05
Northeast
n = 179
y = 0.55x + 0.12
r = 0.74
RMSE = 0.07
MAE = 0.05
Terra Mean = 0.21
MERRA-2 Mean = 0.23
RMB = 0.11
Gobi Desert
n = 173
y = 0.65x + 0.09
r = 0.71
RMSE = 0.12
MAE = 0.09
Terra Mean = 0.31
MERRA-2 Mean = 0.29
RMB = -0.05
Northeast
n = 179
y = 0.25x + 0.33
r = 0.62
RMSE = 0.28
MAE = 0.23
Terra Mean = 0.72
CMIP6 Mean = 0.50
RMB = -0.30
North China
n = 179
y = 0.25x + 0.39
r = 0.45
RMSE = 0.18
MAE = 0.13
Terra Mean = 0.67
CMIP6 Mean = 0.56
RMB = -0.16
Yangtse River Delta
n = 179
y = 0.66x + 0.09
r = 0.89
RMSE = 0.19
MAE = 0.16
Terra Mean = 0.72
MERRA-2 Mean = 0.56
RMB = -0.22
North China
n = 179
y = 0.51x + 0.20
r = 0.66
RMSE = 0.17
MAE = 0.14
Terra Mean = 0.67
MERRA-2 Mean = 0.54
RMB = -0.19
Yangtse River Delta
n = 179
y = 0.21x + 0.54
r = 0.28
RMSE = 0.19
MAE = 0.15
Terra Mean = 0.69
CMIP6 Mean = 0.68
RMB = -0.02
Central
n = 174
y = -0.01x + 0.66
r = -0.02
RMSE = 0.24
MAE = 0.18
Terra Mean = 0.64
CMIP6 Mean = 0.65
RMB = 0.02
Sichuan Basin
n = 179
y = 0.44x + 0.33
r = 0.51
RMSE = 0.18
MAE = 0.14
Terra Mean = 0.69
MERRA-2 Mean = 0.64
RMB = -0.08
Central
n = 174
y = 0.15x + 0.54
r = 0.19
RMSE = 0.23
MAE = 0.19
Terra Mean = 0.64
MERRA-2 Mean = 0.64
RMB = 0.00
Sichuan Basin
n = 178
y = 0.37x + 0.28
r = 0.66
RMSE = 0.15
MAE = 0.12
Terra Mean = 0.54
CMIP6 Mean = 0.48
RMB = -0.12
Pearl River Delta
n = 179
y = 0.04x + 0.21
r = 0.06
RMSE = 0.13
MAE = 0.09
Terra Mean = 0.19
CMIP6 Mean = 0.22
RMB = 0.17
Qinghai
n = 178
y = 0.91x - 0.01
r = 0.85
RMSE = 0.12
MAE = 0.09
Terra Mean = 0.54
MERRA-2 Mean = 0.48
RMB = -0.12
Pearl River Delta
n = 179
y = 0.25x + 0.07
r = 0.53
RMSE = 0.11
MAE = 0.08
Terra Mean = 0.19
MERRA-2 Mean = 0.12
RMB = -0.36
Qinghai
n = 179
y = 0.26x + 0.12
r = 0.38
RMSE = 0.05
MAE = 0.04
Terra Mean = 0.13
CMIP6 Mean = 0.16
RMB = 0.19
Tibetan Plateau
n = 179
y = 0.28x + 0.49
r = 0.33
RMSE = 0.36
MAE = 0.29
Terra Mean = 0.37
CMIP6 Mean = 0.59
RMB = 0.60
Tarim Basin
n = 177
y = 0.50x - 0.00
r = 0.81
RMSE = 0.08
MAE = 0.07
Terra Mean = 0.13
MERRA-2 Mean = 0.06
RMB = -0.53
Tibetan Plateau
n = 179
y = 0.34x + 0.25
r = 0.64
RMSE = 0.20
MAE = 0.15
Terra Mean = 0.37
MERRA-2 Mean = 0.37
RMB = 0.01
Tarim Basin
n = 179
y = 0.34x + 0.25
r = 0.56
RMSE = 0.09
MAE = 0.07
Terra Mean = 0.36
CMIP6 Mean = 0.38
RMB = 0.04
Entire China
n = 179
y = 0.59x + 0.08
r = 0.88
RMSE = 0.08
MAE = 0.07
Terra Mean = 0.36
MERRA-2 Mean = 0.30
RMB = -0.18
Entire China
CMIP6 AOD
MERRA-2 AOD
MODIS DTB AOD
0
0.1
0.2
0.3
0.4
0.5
0.6
0.7
0.8
0.9
1

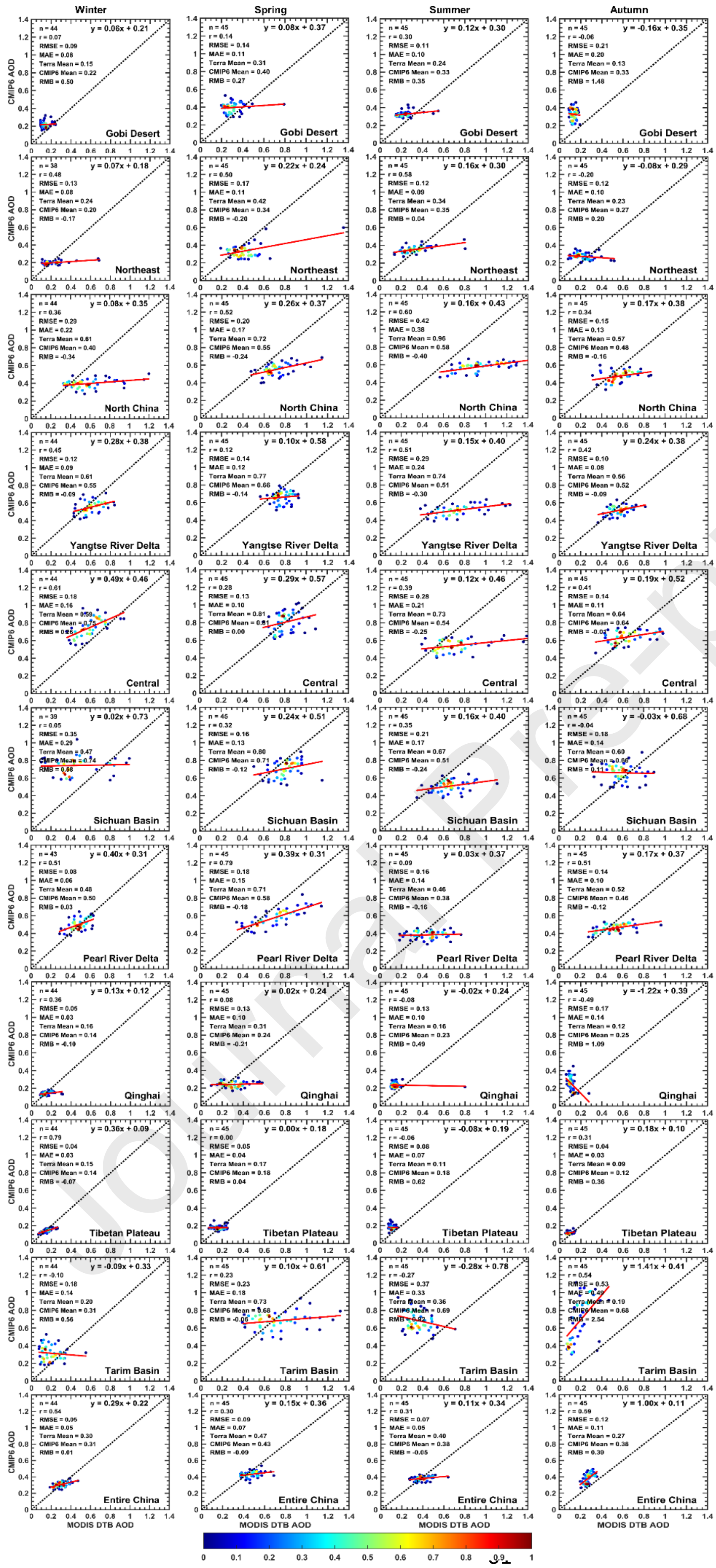

Winter
Spring
Summer
Autumn
CMIP6 AOD
MODIS DTB AOD
Gobi Desert
n = 44 r = 0.07 RMSE = 0.09 MAE = 0.08 Terra Mean = 0.15 CMIP6 Mean = 0.22 RMB = 0.50 y = 0.06x + 0.21
n = 45 r = 0.14 RMSE = 0.14 MAE = 0.11 Terra Mean = 0.31 CMIP6 Mean = 0.40 RMB = 0.27 y = 0.08x + 0.37
n = 45 r = 0.30 RMSE = 0.11 MAE = 0.10 Terra Mean = 0.24 CMIP6 Mean = 0.33 RMB = 0.35 y = 0.12x + 0.30
n = 45 r = -0.06 RMSE = 0.21 MAE = 0.20 Terra Mean = 0.13 CMIP6 Mean = 0.33 RMB = 1.48 y = -0.16x + 0.35
Northeast
n = 38 r = 0.48 RMSE = 0.13 MAE = 0.08 Terra Mean = 0.24 CMIP6 Mean = 0.20 RMB = -0.17 y = 0.07x + 0.18
n = 45 r = 0.50 RMSE = 0.17 MAE = 0.11 Terra Mean = 0.42 CMIP6 Mean = 0.34 RMB = -0.20 y = 0.22x + 0.24
n = 45 r = 0.58 RMSE = 0.12 MAE = 0.09 Terra Mean = 0.34 CMIP6 Mean = 0.35 RMB = 0.04 y = 0.16x + 0.30
n = 45 r = -0.20 RMSE = 0.12 MAE = 0.10 Terra Mean = 0.23 CMIP6 Mean = 0.27 RMB = 0.20 y = -0.08x + 0.29
North China
n = 44 r = 0.36 RMSE = 0.29 MAE = 0.22 Terra Mean = 0.61 CMIP6 Mean = 0.40 RMB = -0.34 y = 0.08x + 0.35
n = 45 r = 0.52 RMSE = 0.20 MAE = 0.17 Terra Mean = 0.72 CMIP6 Mean = 0.55 RMB = -0.24 y = 0.26x + 0.37
n = 45 r = 0.60 RMSE = 0.42 MAE = 0.38 Terra Mean = 0.96 CMIP6 Mean = 0.58 RMB = -0.40 y = 0.16x + 0.43
n = 45 r = 0.34 RMSE = 0.15 MAE = 0.13 Terra Mean = 0.57 CMIP6 Mean = 0.48 RMB = -0.16 y = 0.17x + 0.38
Yangtse River Delta
n = 44 r = 0.45 RMSE = 0.12 MAE = 0.09 Terra Mean = 0.61 CMIP6 Mean = 0.55 RMB = -0.09 y = 0.28x + 0.38
n = 45 r = 0.12 RMSE = 0.14 MAE = 0.12 Terra Mean = 0.77 CMIP6 Mean = 0.66 RMB = -0.14 y = 0.10x + 0.58
n = 45 r = 0.51 RMSE = 0.29 MAE = 0.24 Terra Mean = 0.74 CMIP6 Mean = 0.51 RMB = -0.30 y = 0.15x + 0.40
n = 45 r = 0.42 RMSE = 0.10 MAE = 0.08 Terra Mean = 0.56 CMIP6 Mean = 0.52 RMB = -0.09 y = 0.24x + 0.38
Central
n = 44 r = 0.61 RMSE = 0.18 MAE = 0.16 Terra Mean = 0.59 CMIP6 Mean = 0.75 RMB = 0.26 y = 0.49x + 0.46
n = 45 r = 0.28 RMSE = 0.13 MAE = 0.10 Terra Mean = 0.81 CMIP6 Mean = 0.81 RMB = 0.00 y = 0.29x + 0.57
n = 45 r = 0.39 RMSE = 0.28 MAE = 0.21 Terra Mean = 0.73 CMIP6 Mean = 0.54 RMB = -0.25 y = 0.12x + 0.46
n = 45 r = 0.41 RMSE = 0.14 MAE = 0.11 Terra Mean = 0.64 CMIP6 Mean = 0.64 y = 0.19x + 0.52
Sichuan Basin
n = 39 r = 0.05 RMSE = 0.35 MAE = 0.29 Terra Mean = 0.47 CMIP6 Mean = 0.74 y = 0.02x + 0.73
n = 45 r = 0.32 RMSE = 0.16 MAE = 0.13 Terra Mean = 0.80 CMIP6 Mean = 0.71 RMB = -0.12 y = 0.24x + 0.51
n = 45 r = 0.35 RMSE = 0.21 MAE = 0.17 Terra Mean = 0.67 CMIP6 Mean = 0.51 RMB = -0.24 y = 0.16x + 0.40
n = 45 r = -0.04 RMSE = 0.18 MAE = 0.14 Terra Mean = 0.60 RMB = 0.11 y = -0.03x + 0.68
Pearl River Delta
n = 43 r = 0.51 RMSE = 0.08 MAE = 0.06 Terra Mean = 0.48 CMIP6 Mean = 0.50 RMB = 0.03 y = 0.40x + 0.31
n = 45 r = 0.79 RMSE = 0.18 MAE = 0.15 Terra Mean = 0.71 CMIP6 Mean = 0.58 RMB = -0.18 y = 0.39x + 0.31
n = 45 r = 0.09 RMSE = 0.16 MAE = 0.14 Terra Mean = 0.46 CMIP6 Mean = 0.38 RMB = -0.16 y = 0.03x + 0.37
n = 45 r = 0.51 RMSE = 0.14 MAE = 0.10 Terra Mean = 0.52 CMIP6 Mean = 0.46 RMB = -0.12 y = 0.17x + 0.37
Qinghai
n = 44 r = 0.36 RMSE = 0.05 MAE = 0.03 Terra Mean = 0.16 CMIP6 Mean = 0.14 RMB = -0.10 y = 0.13x + 0.12
n = 45 r = 0.08 RMSE = 0.13 MAE = 0.10 Terra Mean = 0.31 CMIP6 Mean = 0.24 RMB = -0.21 y = 0.02x + 0.24
n = 45 r = -0.08 RMSE = 0.13 MAE = 0.10 Terra Mean = 0.16 CMIP6 Mean = 0.23 RMB = 0.49 y = -0.02x + 0.24
n = 45 r = -0.49 RMSE = 0.17 MAE = 0.14 Terra Mean = 0.12 CMIP6 Mean = 0.25 RMB = 1.09 y = -1.22x + 0.39
Tibetan Plateau
n = 44 r = 0.79 RMSE = 0.04 MAE = 0.03 Terra Mean = 0.15 CMIP6 Mean = 0.14 RMB = -0.07 y = 0.36x + 0.09
n = 45 r = 0.06 RMSE = 0.05 MAE = 0.04 Terra Mean = 0.17 CMIP6 Mean = 0.18 RMB = 0.04 y = 0.00x + 0.18
n = 45 r = -0.06 RMSE = 0.08 MAE = 0.07 Terra Mean = 0.11 CMIP6 Mean = 0.18 RMB = 0.62 y = -0.08x + 0.19
n = 45 r = 0.31 RMSE = 0.04 MAE = 0.03 Terra Mean = 0.09 CMIP6 Mean = 0.12 RMB = 0.36 y = 0.18x + 0.10
Tarim Basin
n = 44 r = -0.10 RMSE = 0.18 MAE = 0.14 Terra Mean = 0.20 CMIP6 Mean = 0.31 RMB = 0.56 y = -0.09x + 0.33
n = 45 r = 0.23 RMSE = 0.23 MAE = 0.18 Terra Mean = 0.73 CMIP6 Mean = 0.68 y = 0.10x + 0.61
n = 45 r = -0.27 RMSE = 0.37 MAE = 0.33 Terra Mean = 0.36 CMIP6 Mean = 0.69 y = -0.28x + 0.78
n = 45 r = 0.54 RMSE = 0.53 MAE = 0.49 Terra Mean = 0.19 CMIP6 Mean = 0.68 RMB = 2.54 y = 1.41x + 0.41
Entire China
n = 44 r = 0.54 RMSE = 0.05 MAE = 0.05 Terra Mean = 0.30 CMIP6 Mean = 0.31 RMB = 0.01 y = 0.29x + 0.22
n = 45 r = 0.30 RMSE = 0.09 MAE = 0.07 Terra Mean = 0.47 CMIP6 Mean = 0.43 RMB = -0.09 y = 0.15x + 0.36
n = 45 r = 0.31 RMSE = 0.07 MAE = 0.05 Terra Mean = 0.40 CMIP6 Mean = 0.38 RMB = -0.05 y = 0.11x + 0.34
n = 45 r = 0.59 RMSE = 0.12 MAE = 0.11 Terra Mean = 0.27 CMIP6 Mean = 0.38 RMB = 0.39 y = 1.00x + 0.11
0 0.1 0.2 0.3 0.4 0.5 0.6 0.7 0.8 0.9 1

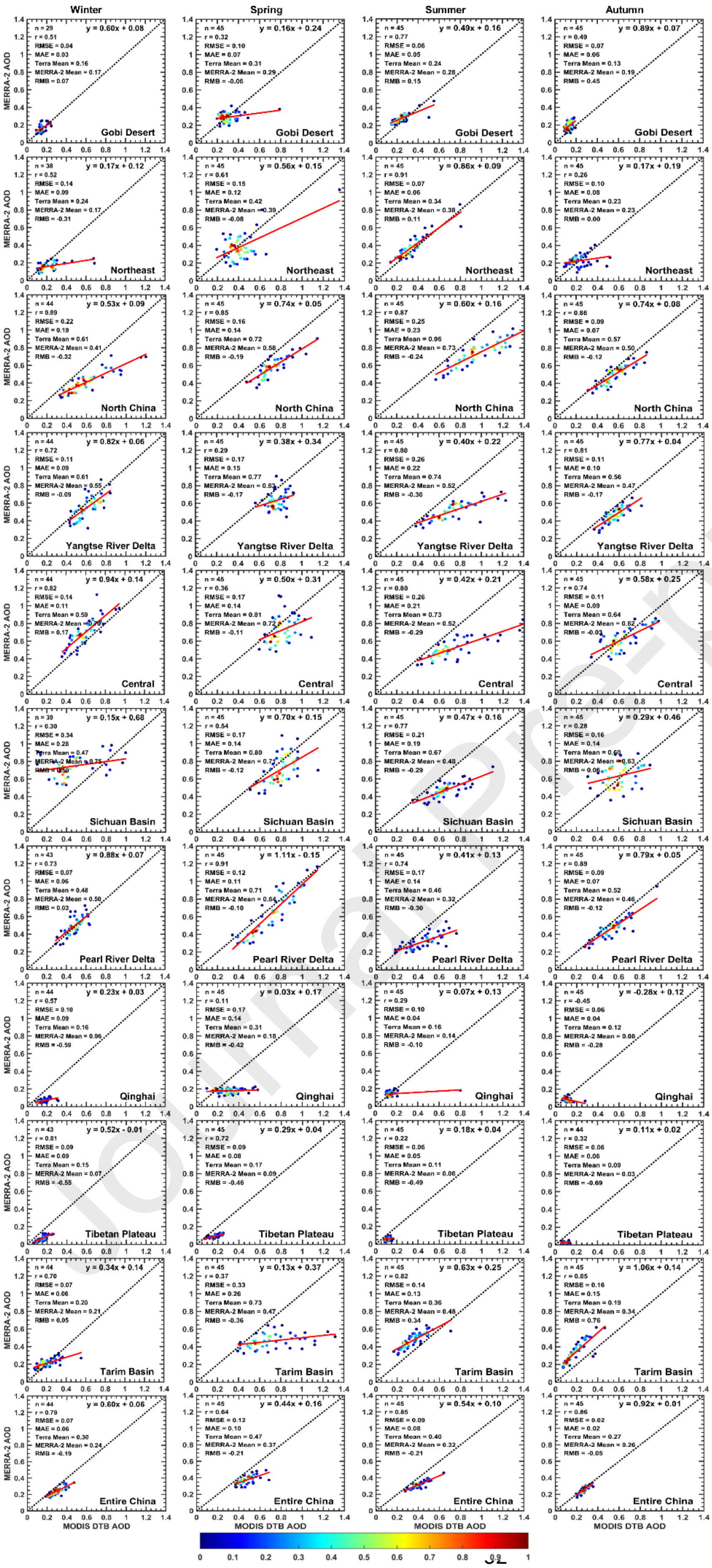
Winter
Spring
Summer
Autumn
MERRA-2 AOD
MODIS DTB AOD
y = 0.60x + 0.08
y = 0.16x + 0.24
y = 0.49x + 0.16
y = 0.89x + 0.07
Gobi Desert
y = 0.17x + 0.12
y = 0.56x + 0.15
y = 0.86x + 0.09
y = 0.17x + 0.19
Northeast
y = 0.53x + 0.09
y = 0.74x + 0.05
y = 0.60x + 0.16
y = 0.74x + 0.08
North China
y = 0.82x + 0.06
y = 0.38x + 0.34
y = 0.40x + 0.22
y = 0.77x + 0.04
Yangtse River Delta
y = 0.94x + 0.14
y = 0.50x + 0.31
y = 0.42x + 0.21
y = 0.58x + 0.25
Central
y = 0.15x + 0.68
y = 0.70x + 0.15
y = 0.47x + 0.16
y = 0.29x + 0.46
Sichuan Basin
y = 0.88x + 0.07
y = 1.11x - 0.15
y = 0.41x + 0.13
y = 0.79x + 0.05
Pearl River Delta
y = 0.23x + 0.03
y = 0.03x + 0.17
y = 0.07x + 0.13
y = -0.28x + 0.12
Qinghai
y = 0.52x - 0.01
y = 0.29x + 0.04
y = 0.18x + 0.04
y = 0.11x + 0.02
Tibetan Plateau
y = 0.34x + 0.14
y = 0.13x + 0.37
y = 0.63x + 0.25
y = 1.06x + 0.14
Tarim Basin
y = 0.60x + 0.06
y = 0.44x + 0.16
y = 0.54x + 0.10
y = 0.92x + 0.01
Entire China

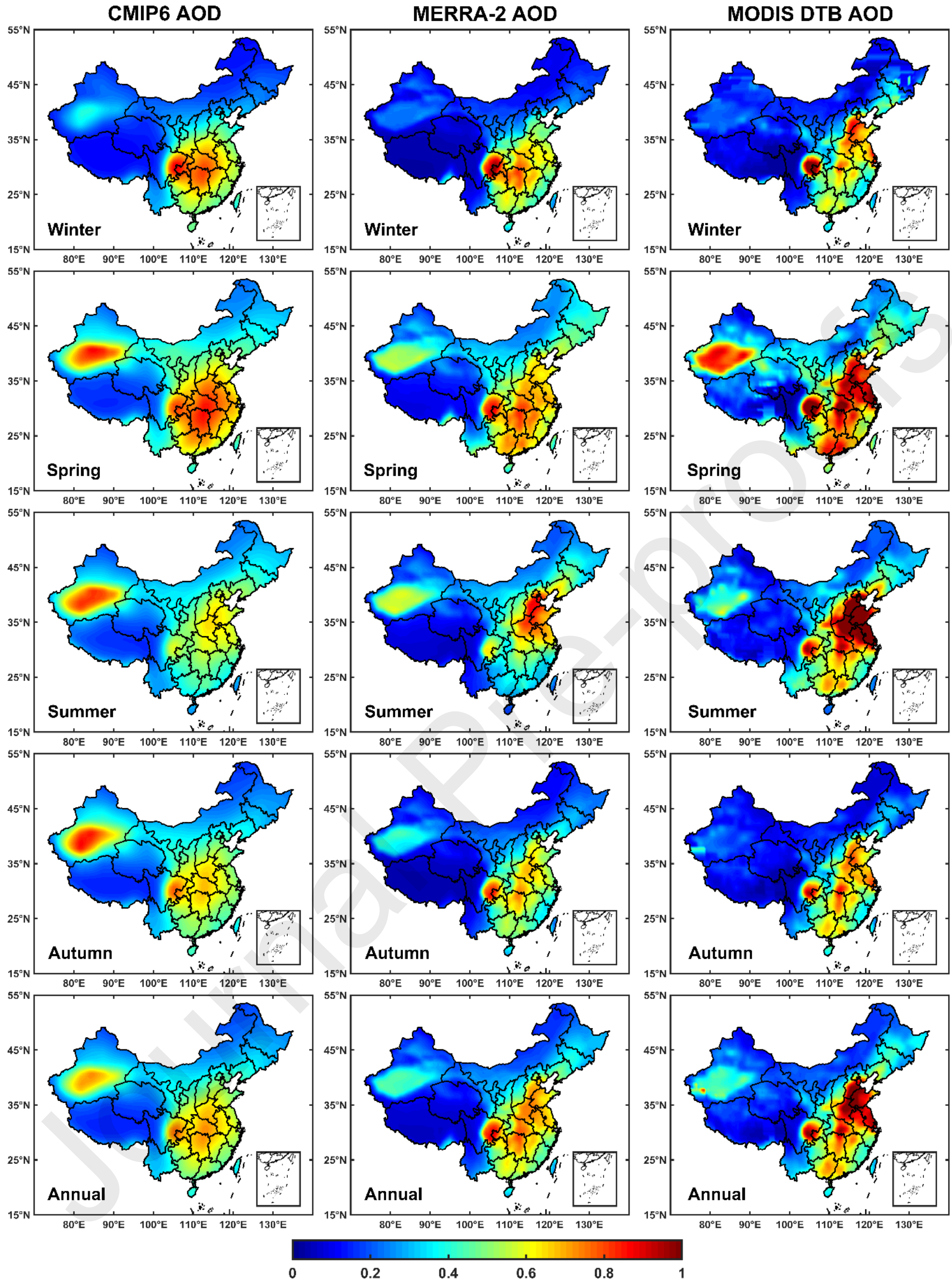
CMIP6 AOD
MERRA-2 AOD
MODIS DTB AOD
Winter
Spring
Summer
Autumn
Annual
55°N
45°N
35°N
25°N
15°N
80°E
90°E
100°E
110°E
120°E
130°E
0
0.2
0.4
0.6
0.8
1

1217

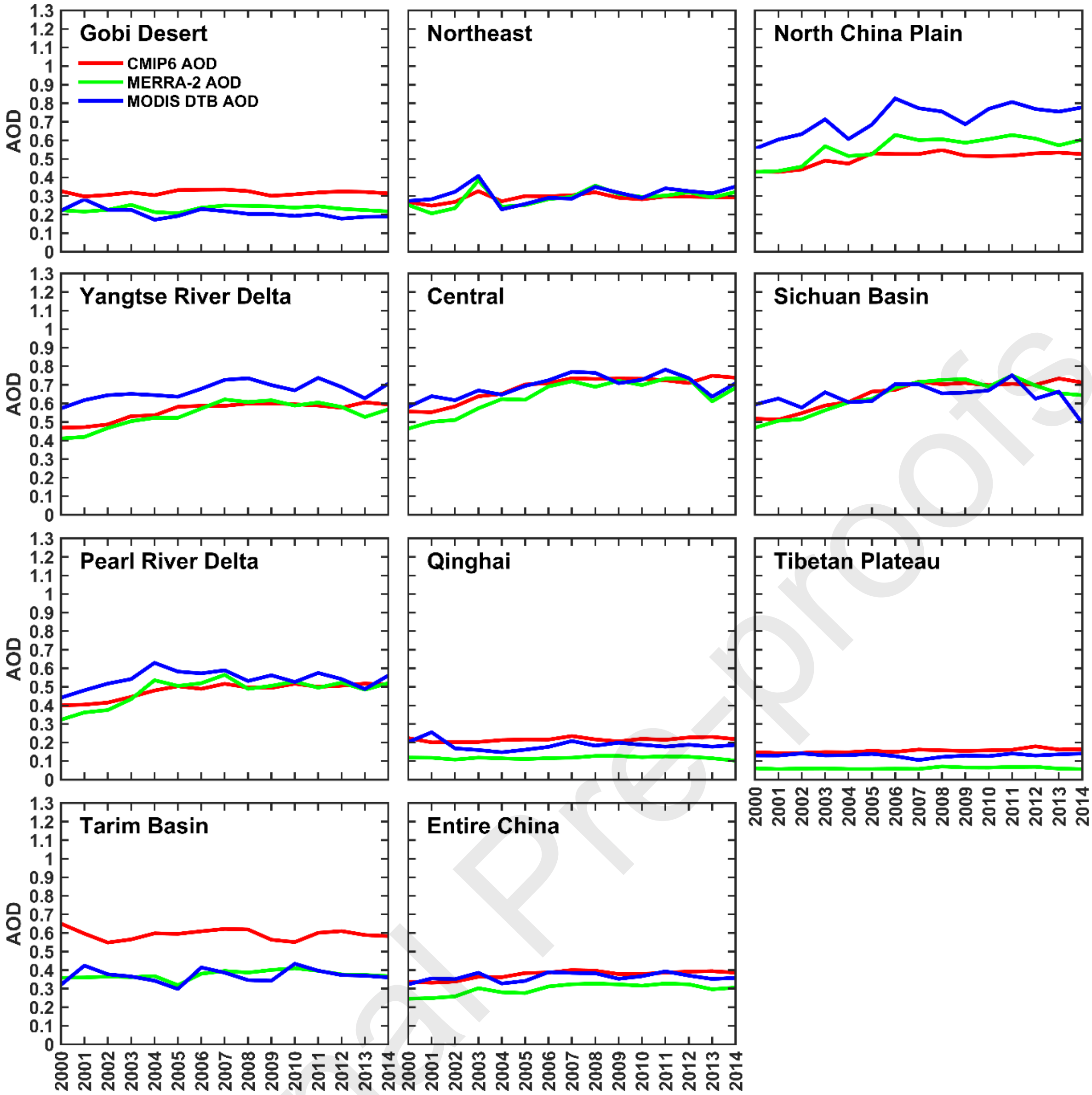
Gobi Desert
CMIP6 AOD
MERRA-2 AOD
MODIS DTB AOD
Northeast
North China Plain
Yangtse River Delta
Central
Sichuan Basin
Pearl River Delta
Qinghai
Tibetan Plateau
Tarim Basin
Entire China
AOD

1218

1219 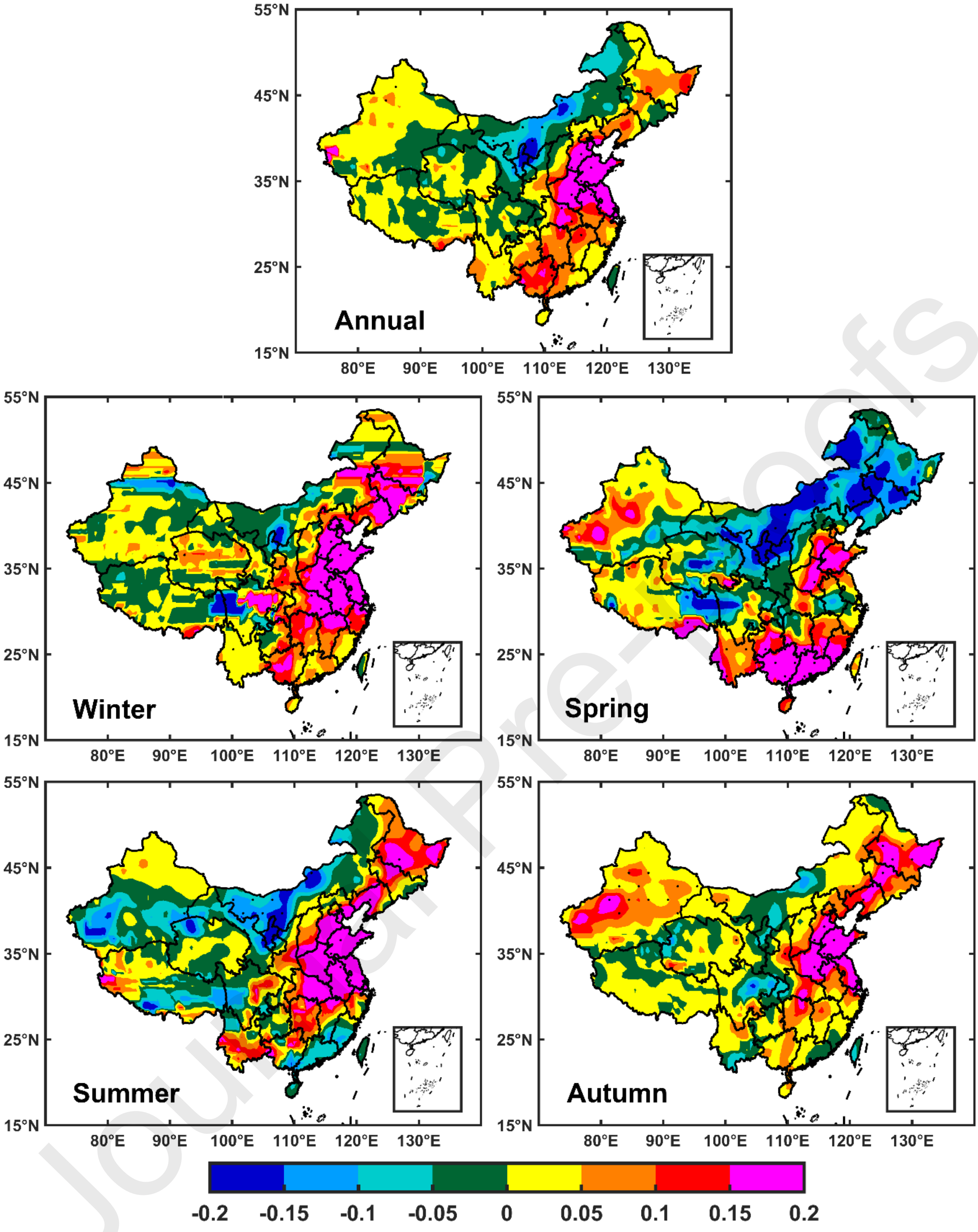
Annual
Winter
Spring
Summer
Autumn
55°N
45°N
35°N
25°N
15°N
80°E
90°E
100°E
110°E
120°E
130°E
-0.2
-0.15
-0.1
-0.05
0
0.05
0.1
0.15
0.2

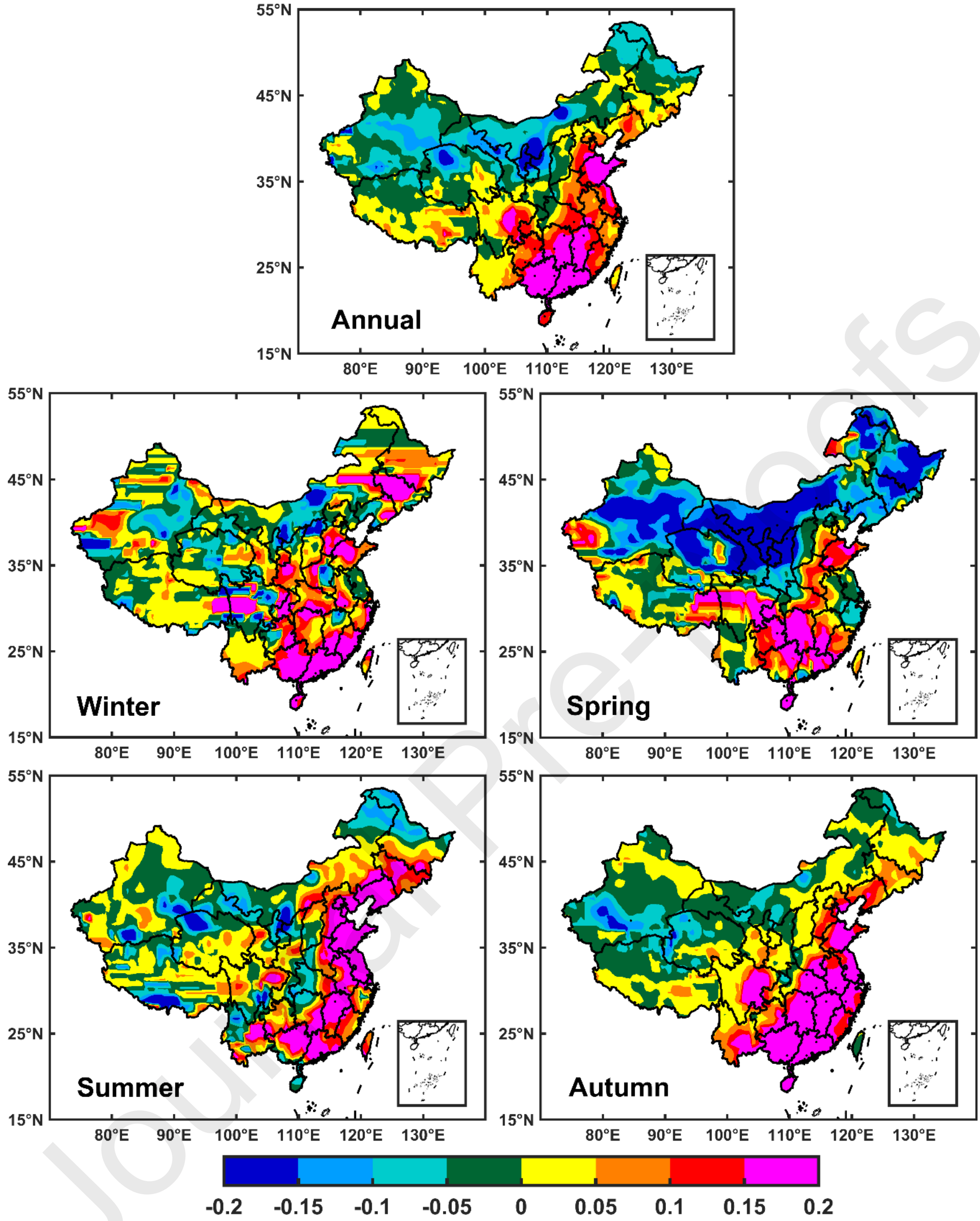

Annual
Winter
Spring
Summer
Autumn
55°N
45°N
35°N
25°N
15°N
80°E
90°E
100°E
110°E
120°E
130°E
-0.2
-0.15
-0.1
-0.05
0
0.05
0.1
0.15
0.2

1220

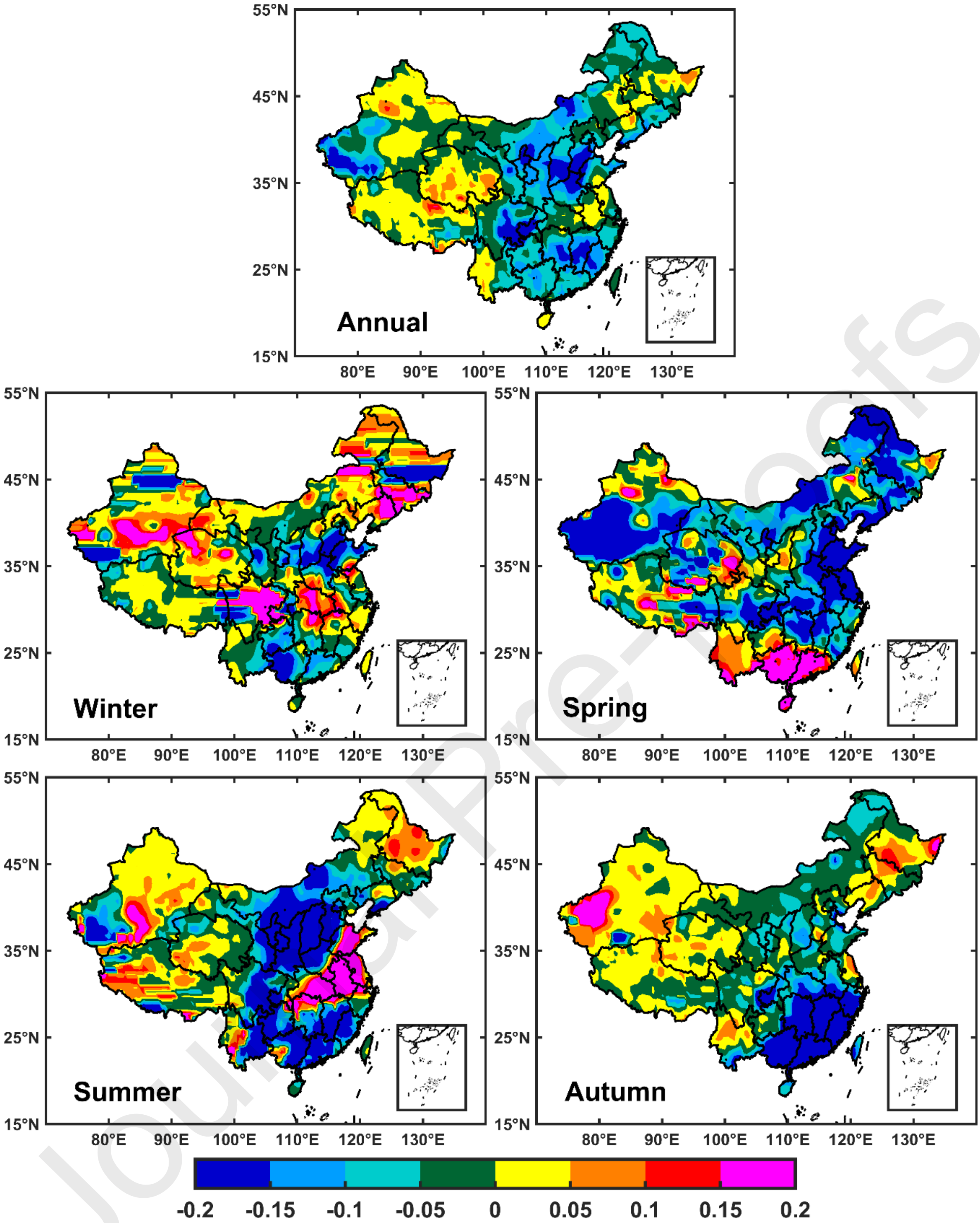
Annual
Winter
Spring
Summer
Autumn
55°N
45°N
35°N
25°N
15°N
80°E
90°E
100°E
110°E
120°E
130°E
-0.2
-0.15
-0.1
-0.05
0
0.05
0.1
0.15
0.2

1221

1222 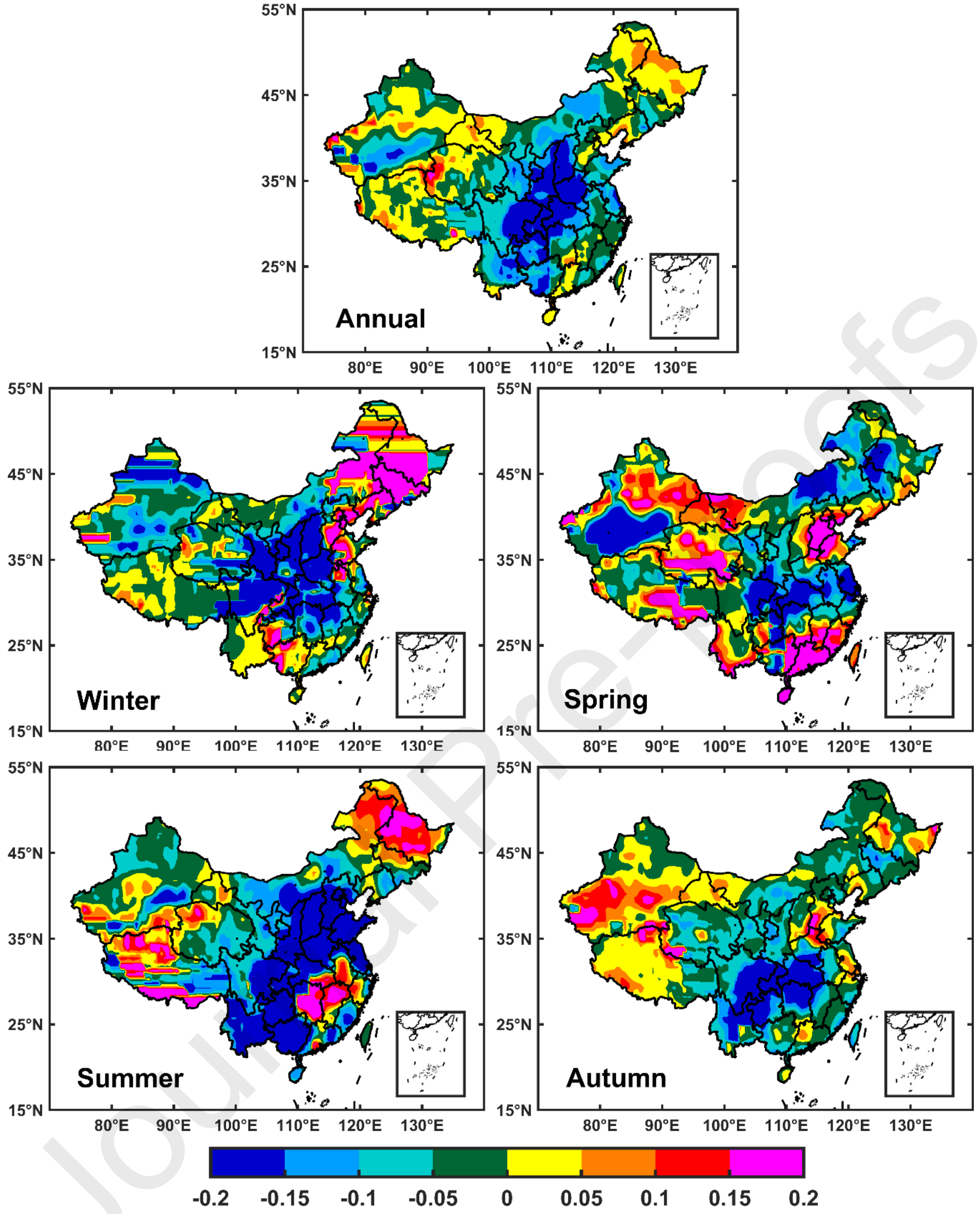
Annual
Winter
Spring
Summer
Autumn
55°N
45°N
35°N
25°N
15°N
80°E
90°E
100°E
110°E
120°E
130°E
-0.2
-0.15
-0.1
-0.05
0
0.05
0.1
0.15
0.2

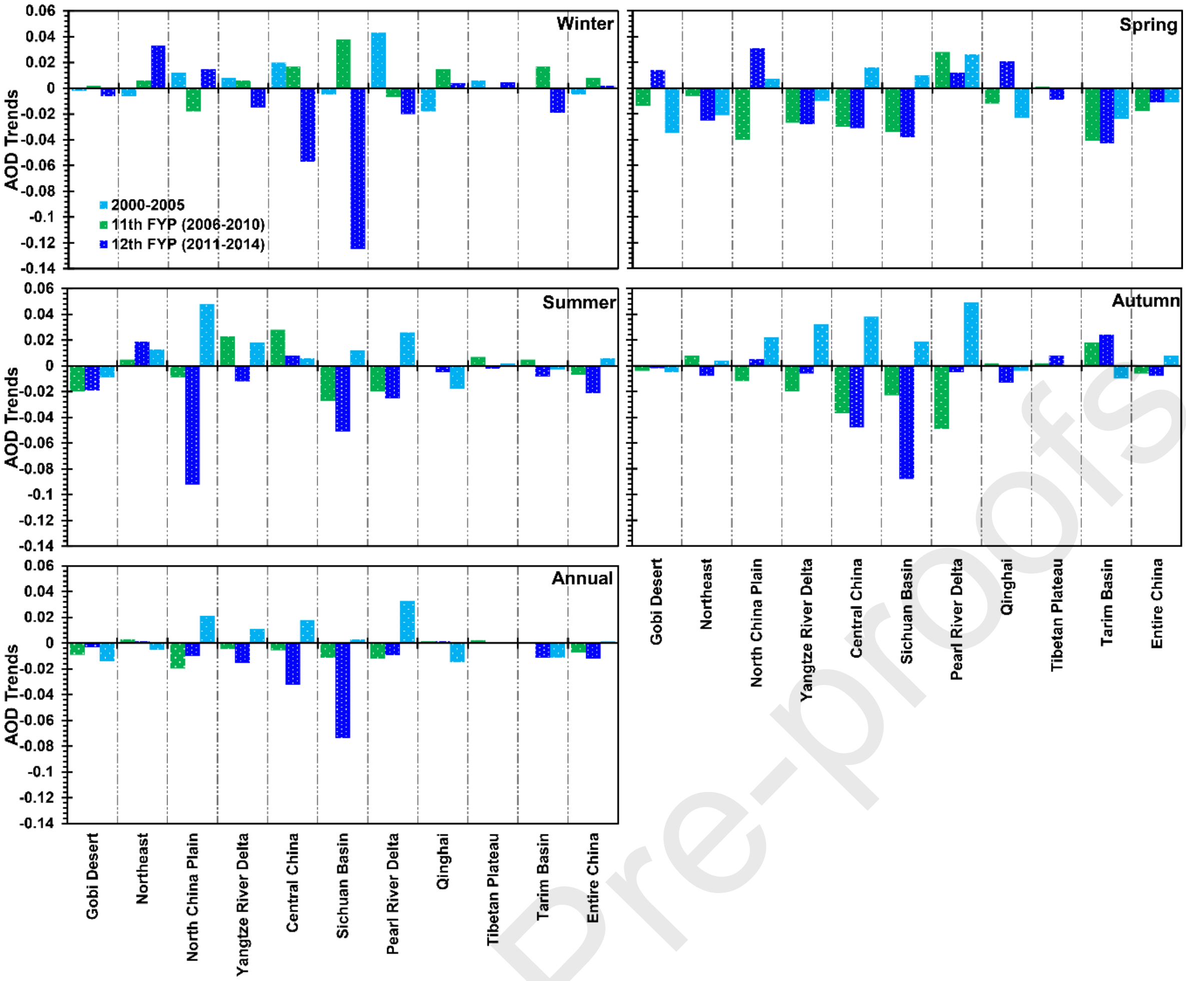
Winter
Spring
Summer
Autumn
Annual
AOD Trends
2000-2005
11th FYP (2006-2010)
12th FYP (2011-2014)
0.06
0.04
0.02
0
-0.02
-0.04
-0.06
-0.08
-0.1
-0.12
-0.14
Gobi Desert
Northeast
North China Plain
Yangtze River Delta
Central China
Sichuan Basin
Pearl River Delta
Qinghai
Tibetan Plateau
Tarim Basin
Entire China

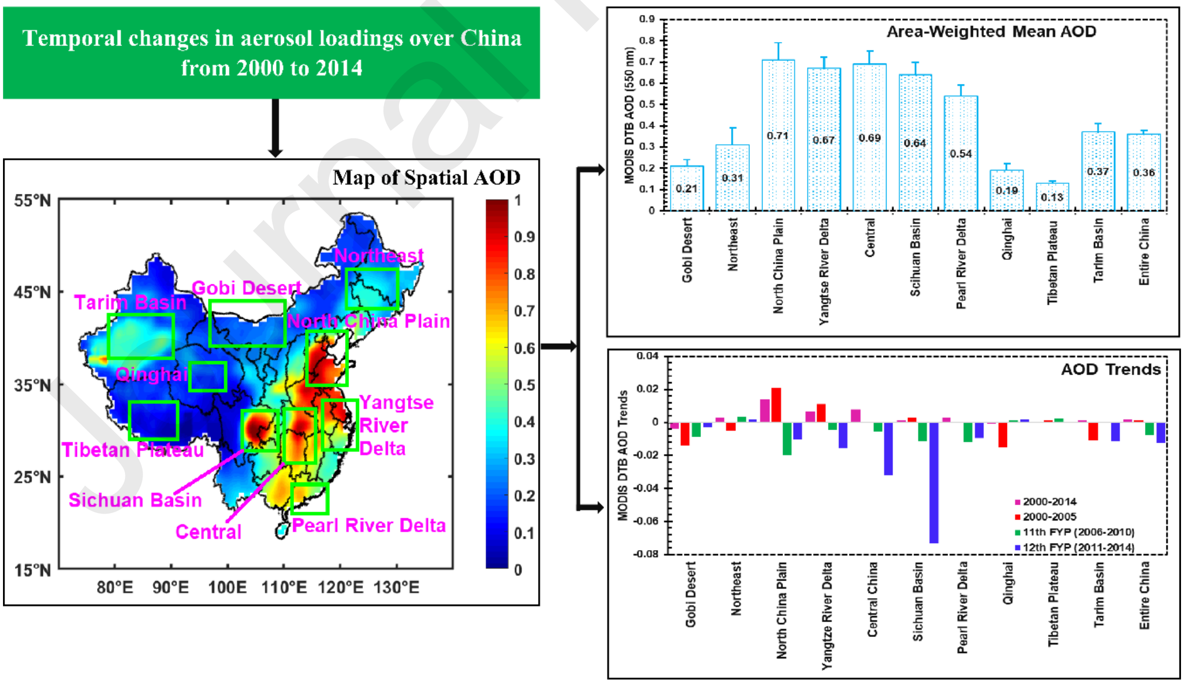
Temporal changes in aerosol loadings over China from 2000 to 2014
Map of Spatial AOD
55°N
45°N
35°N
25°N
15°N
80°E
90°E
100E
110°E
120°E
130°E
Tarim Basin
Gobi Desert
Northeast
North China Plain
Qinghai
Tibetan Plateau
Yangtse River Delta
Sichuan Basin
Central
Pearl River Delta
Area-Weighted Mean AOD
MODIS DTB AOD (550 nm)
0.21
0.31
0.71
0.67
0.69
0.64
0.54
0.19
0.13
0.37
0.36
AOD Trends
MODIS DTB AOD Trends
2000-2014
2000-2005
11th FYP (2006-2010)
12th FYP (2011-2014)
Gobi Desert
Northeast
North China Plain
Yangtse River Delta
Central
Central China
Sichuan Basin
Pearl River Delta
Qinghai
Tibetan Plateau
Tarim Basin
Entire China

Highlights:

- The CMIP6 and MERRA-2 were not in line with Terra-MODIS DTB
- AOD upward trends were found during 2000–2014 and 2000–2005
- China's strict air pollution control policies had co-benefits to reduce AOD
- AOD reduction was more prominent during the 12^{th} FYP than the 11^{th} FYP period
- Seasonally, AOD decrease was more prominent in summer during the 12^{th} FYP period